SUPPLEMENTAL MATERIAL

for

Insulin Receptor Substrates Differentially Exacerbate Insulin-Mediated Left Ventricular Remodeling

Christian Riehle, Eric T. Weatherford, Adam R. Wende, Bharat P. Jaishy, Alec W. Seei, Nicholas S. McCarty, Monika Rech, Qian Shi, Gopireddy R. Reddy, William J. Kutschke, Karen Oliveira, Karla Maria Pires, Joshua C. Anderson, Nikolaos A. Diakos, Robert M. Weiss, Morris F. White, Stavros G. Drakos, Yang K. Xiang, E. Dale Abel

Supplemental Methods

Transverse aortic constriction (TAC)

In our early studies, TAC procedures were performed on mice at 6 weeks of age and a titanium clip calibrated to the diameter of a 30-G needle was placed between the innominate artery and the left common carotid artery as previously described. The Sham procedure was performed identically, except no clip was placed around the aortic arch (1). We subsequently modified our protocol to tighten a 7-0 Prolene suture around a blunt 27-G needle, which was placed between the innominate artery and the left common carotid artery (2). Mice subjected to this protocol have been investigated for a maximum duration of 2 weeks. Mice for the 2-day and 3-day time point were operated at the age of 6 weeks and for the 2-week time point at 8 weeks of age. These data are presented in Figures 1D-G, 6, 7, Supplemental Figures 1E, 6, 7 and Supplemental Tables 1 and 3. All other data were generated using our previous surgery protocol. Both surgery protocols resulted in a similar increase in the pressure gradient following TAC, which was independent of the genotype (Supplemental Figure 1). Invasive measurements using left ventricular (LV) catheterization showed no difference in LV systolic pressure and LV developed pressure under Sham conditions between the genotypes (Supplemental Table 4). Furthermore, we observed equivalent increase in mean arterial pressure proximal to the band, four weeks post-TAC, which was independent of the genotype (data not shown). Even though not directly measured, these data indicate that TAC resulted in a similar increase in workload independent of the genotype.

Transthoracic echocardiography

Echocardiographic data obtained from sedated CIRS1KO and CIRS2KO mice (depicted in Supplemental Table 2) were acquired and calculated as follows: Anesthesia was induced with 3% isoflurane and followed by maintenance at 1 to 2%. Mice were placed on a heating pad (37 °C), chest hair was removed with a depilatory agent and pre-warmed ultrasonic gel was applied. Echocardiographs immediately post-surgery (indicated as 0 week time point in Supplemental Table 2 and presented in Supplemental Figure 1C/D) was performed with isoflurane anesthesia. B-mode images in parasternal long- and short-axis projections (at the papillary muscle level) were obtained using a Vivid 7 Pro ultrasound machine with a 13 MHz linear probe (GE Medical Systems, Milwaukee, WI). M-mode recordings were obtained in both views (2). Fractional shortening [%] was calculated as [(LVDd - LVDs) / LVDd] * 100, where LVDd = LV diastolic dimension and LVDs = LV systolic dimension. Ejection fraction [%] was calculated as $[(LVDd^3 - LVDs^3) / LVDd^3] * 100$.

Data from CIRS2KO x Akt1^{het} cross experiments (presented in Figure 3D/E and in Supplemental Table 6) were acquired using the same isoflurane anesthesia protocol and a Vevo 660 ultrasound machine with a 40 MHz linear probe (VisualSonics Inc., Toronto, Ontario, Canada). B-mode images were obtained in both parasternal long- and short-axis projections (at the papillary muscle level). M-mode images were generated from short axis projections and were used to measure LV dimensions. Ejection fraction and fractional shortening was determined by speckle tracking of the LV endocardium in long axis view using VevoStrain software (3).

We subsequently modified our protocol to perform echocardiograms on non-sedated mice using a Vevo 2100 ultrasound machine (VisualSonics Inc.) as previously described (4). These data are presented in Figures 1D-G and Supplemental Table 1. Chest hair of the mice was removed with a depilatory agent the day before the echocardiographic examination. Non-sedated conscious mice were grasped gently by the nape of the neck and cradled in the investigator's left hand, approximating a left lateral recumbent position. Echocardiography was performed at 2-days, 2-weeks and 4-weeks post-TAC. We observed variability in some echocardiographic parameters in the Sham groups at 2-days, which were not present at 2-weeks or 4-weeks, which may reflect physiological responses in the immediate post-op period and acclimation of mice to repeated echocardiography at later time points. Pre-warmed acoustic gel was applied to the mouse's chest. Two-dimensional B-mode images were acquired in parasternal long- and short-axis planes using a high-resolution MS400 transducer coupled to a Vevo 2100 echocardiograph (VisualSonics Inc.,). In mice, orientation of the heart near-parallel to the spine affords visualization of the entire length of the left ventricle, from a parasternal vantage point. Short-axis frames were acquired at the level of the chordae tendineae. End-diastole was visually identified in each plane as the echocardiographic frame where LV endocardial area was greatest. End-systole was visually identified as the frame where LV endocardial area was least. Short-axis endocardial silhouettes were traced manually, yielding short-axis endocardial area at end-diastole and end-systole. LV long-axis length was measured between the endocardial apex and the mid-point of the aortic valve annulus, at end-diastole and end-systole. LV blood volumes were calculated using the following established formula: Volume = 0.833 * (short-axis area) * (long-axis length).

This convention was employed because it provides accurate echocardiographic quantitation of LV mass, where postmortem LV wet weight was used as the reference standard (5). Because echocardiographic calculations of LV mass were based on measurements of both endocardial and epicardial measurements of area-length, accuracy of the endocardial measurements performed here, in the same fashion, is strongly inferred. Ejection fraction [%] was calculated

as (EDV - ESV) / EDV, where EDV = LV end-diastolic volume and ESV = LV end-systolic volume. Heart rate was determined by measuring the time required to complete a cardiac cycle, averaged over three consecutive beats.
All echocardiographic images were generated and analyzed by investigators blinded to genotype and surgery condition.

Measurement of TAC-induced pressure gradient

Measurement of carotid artery peak velocity

Doppler peak velocity of the right and left carotid artery was determined using a 13 MHz Doppler probe immediately post-surgery. The peak flow velocity difference of the right / left carotid artery was used to determine the TAC-induced pressure gradient (Clip method) (2, 6, 7). Transthoracic echocardiography showed no difference in contractile function and heart rate at this early time point between the genotypes (Supplemental Table 2 and Supplemental Figure 1C/D).

Measurement of trans-TAC pressure gradient

Measurements were performed one day post TAC-surgery (suture method) following anesthesia with isoflurane (4). The transverse aorta was visualized by transthoracic echocardiography and transverse aortic velocity distal to the constriction was determined by pulsed-wave Doppler measurement. The pressure gradient was estimated by applying the modified Bernoulli equation (Maximum pressure gradient = $4 * V_{max}^2$, where V_{max} = peak velocity distal the TAC-induced stenosis) (8).

Hemodynamic studies

Mice were anesthetized (single intraperitoneal injection of 400 mg chloral hydrate / kg body weight) and placed in the supine position on a heating pad (37 °C). The right carotid artery was accessed by the cut down method. Next, a 1.4-F micromanometer-tipped pressure catheter (Millar Instruments, Houston, TX) was inserted and retrogradely introduced into the left ventricle. Hemodynamic measurements were obtained using LabChart7 Pro software (ADInstruments, Colorado Springs, CO) (2).

Histology and stereological quantification

Myocardial fragments were embedded in paraffin, portioned into 3 µm-thick sections and stained with hematoxylin-eosin (Fisher, Pittsburgh, PA) or Masson's trichrome (Sigma-Aldrich, St. Louis, MO). Light microscopy was performed using an Olympus LX81 inverted microscope that was connected to an Olympus Microfire Digital Camera (New York, NY). From

each sample, ten microscopic fields of myocardial sections were analyzed at random with a 36-point test-system, the stage of the microscope being moved blindly.

For stereological quantification, the number of cardiomyocyte nuclei detected was normalized to the test area. Volume density (V_v) of cardiomyocytes ($V_{v\ [CMY]}$) and interstitium ($V_{v\ [Int]}$) was estimated as follows: $V_{v\ [Structure]} = P_{P\ [Structure]} / P_T$, where $P_{P\ [Structure]}$ is the number of points that hit the structure and P_T is the total number of test-points inside the frame. Mean cross-sectional area of cardiomyocytes $A_{[CMY]}$ was estimated as follows: $A_{[CMY]} = V_{v\ [CMY]} / 2Q_{A\ [CMY]}$; where $Q_{A\ [CMY]} = n_{[CMY]} / A_T$; $n_{[CMY]}$ is the number of cardiomyocyte profiles counted in the test frame area, and A_T is the test frame area considering the forbidden line and its extensions (9).

Immunoprecipitation

Total protein extraction was performed as previously reported (2). For Akt isoform-specific immunoprecipitation, 500 µg of protein extracts were incubated with 5 µg of anti-Akt1 or anti-Akt2 antibodies (Cell Signaling, Danvers, MA) for 3 h at constant agitation at 4 °C, agarose beads (Millipore Corp., Billerica, MA) were added, incubated for 1 h, and washed four times. Immune complexes were resuspended in 30 µl of 2x SDS sample buffer containing 5% ß-Mercaptoethanol and were incubated for 5 min at 95 °C. Next, samples were centrifuged for 1 min at 8,000 g and subjected to immunoblotting analysis with antibodies to Ser473/474 and Thr308/309 of Akt1 and Akt2 respectively.

Immunoblotting

Total protein extraction was performed as previously reported (2). Proteins were resolved by SDS-PAGE and electrotransferred to nitrocellulose (IRS proteins, P-mTOR and total mTOR) or PVDF membranes (other targets). Primary antibodies used are summarized in the table below. Protein detection was carried out with anti-Rabbit 680 (Invitrogen, Carlsbad CA), anti-Mouse 680 (VWR International, West Chester, PA) and anti-Mouse 800 (VWR) as secondary antibodies, and fluorescence was quantified using the LI-COR Odyssey imager (Lincoln, NE).

Antigen	Company	Catalog number
4E-BP1	Abcam, Cambridge, MA	2606
Akt1	Cell Signaling, Danvers, MA	2938
Akt2	Cell Signaling, Danvers, MA	3063
GAPDH	Cell Signaling, Danvers, MA	2118
IRS1	Millipore, Billerica MA	06-248
IRS2	Millipore, Billerica MA	06-506
P-4E-BP1 Thr37/46	Cell Signaling, Danvers, MA	2855
P-Akt Ser473	Cell Signaling, Danvers, MA	9271
P-Akt Thr308	Cell Signaling, Danvers, MA	9275
PDE9A	Millipore, Billerica MA	ABN32
P-eNOS Ser1177	Cell Signaling, Danvers, MA	9571
P-FoxO3a Ser318/321	Cell Signaling, Danvers, MA	9465
PKG1	Cell Signaling, Danvers, MA	3248
P-mTOR Ser2448	Cell Signaling, Danvers, MA	2971
P-S6 Ser235/236	Cell Signaling, Danvers, MA	2211
P-Troponin I Ser23/24	Cell Signaling, Danvers, MA	4004
Total Akt	Cell Signaling, Danvers, MA	2920
Total eNOS	BD Biosciences, San Jose CA	610297
Total FoxO3a	Santa Cruz Biotechnology, Dallas, TX	9813
Total mTOR	Cell Signaling, Danvers, MA	4517
Total S6	Cell Signaling, Danvers, MA	2317
Total Troponin I	Cell Signaling, Danvers, MA	13083

Kinomic profiling

Tissue preparation and kinomic analysis

LV tissue obtained four weeks post-surgery was prepared as previously described and subjected to serine-threonine kinome (STK) and tyrosine kinome (PTK) profiling analysis (10). Kinomic profiling was performed using the PamStation®12 platform (PamGene, s-Hertogenbosch, Netherlands) at the University of Alabama, Birmingham, Kinome Core facility (www.kinomecore.com). PamChips® were used that contained 144 individual serine-threonine phosphorylatable peptides (STK) or 144 tyrosine phosphorylatable peptides (PTK) that were immobilized in the chip. After blocking with 2% bovine serum albumin (BSA), lysates were dissolved in manufacturer's kinase buffer (PamGene) and loaded (2 µg/well for STK or 15 µg/well for PTK), and exogenous ATP was added together with FITC-labeled anti-phospho serine-threonine antibodies (STK) or anti-phospho tyrosine antibodies (PTK). Peptide phosphorylation signal was detected in real time by capturing the binding of FITC-labeled anti-phospho serine-threonine antibodies (STK) or anti-phospho tyrosine antibodies (PTK) to each phosphorylated peptide substrate with images captured approximately every 5.5 minutes over the total duration of 50 (STK) or 70 (PTK) minutes, followed by multiple exposure captures over 10 minutes. Signal intensities for each peptide were analyzed using the BioNavigator software package (PamGene) (11).

Data Analysis

Briefly, signal over multiple exposure times (10, 20, 50, 100, and 200 ms) was linearly integrated for each sample and peptide. The slope was log2 transformed as described previously (12). These data were used as 'Signal' for further analysis, and for heat map display (Supplemental Table 9). Peptides were compared using unpaired Student's t tests between experimental conditions. Significantly altered ($p<0.05$) peptides were then mapped for upstream kinases using a modified query of the Kinexus database, which scored each kinase based on the percentage of times it occurred, in a phosphorylatable-residue-corrected manner, within the top 10 list for each phosphorylatable peptide as before (10). Upstream kinases were then uploaded by UniProt ID to GeneGo MetaCore (portal.genego.com) and mapped using the Shortest Paths (2-step) network model without filters for tissue or species to identify literature annotated interactions between the kinases (seed nodes).

RNA sequencing analysis

RNA sequencing was done by the Iowa Institute of Human Genetics: Genomics Division at the University of Iowa. Using the Illumina TruSeq Stranded mRNA sample preparation kit, thirty-six libraries (Illumina, Inc., San Diego, CA) were prepared following Illumina's sample preparation guide. The Illumina Library Quantification Kit (KAPA Biosystems, Wilmington, MA) was used to measure molar concentrations of the indexed libraries and combined equally into one pool. Molar concentration of the pool was measured and sequenced on the Illumina HiSeq 2000 sequencer with a 100 bp Paired-End SBS chemistry (Illumina). Sequences were aligned to the mouse genome (GRCm38/mm10) using HISAT2 (hierarchical indexing for spliced alignment of transcripts). Reads were counted using HTSeq and differential gene expression analysis performed using DESeq2 (13, 14). Significantly regulated genes were defined as those with a fold change greater than 1.5 and adjusted p-value ≤ 0.05. Enrichment for pathways and upstream regulators in each data set was performed using Ingenuity Pathway Analysis (IPA; QIAGEN, Germantown, MD). Predictions on pathway or regulator activation or inhibition determined by IPA were made by assessing the correlation between the directional changes in gene expression and what is known in the literature.

Quantitative RT-PCR

RNA from cardiac tissue was extracted and quantitative real-time PCR analysis was performed using SYBR Green I and ROX internal reference. The following primers were used for quantification of mRNA levels by RT-PCR:

Gene Name **Gene Sequence of forward and reverse primers (5'→ 3')** **GenBank Accession Number**
Actin, alpha 1, skeletal muscle *(Acta1)* CCTGTATGCCAACAACGTCA CTCGTCGTACTCCTGCTTGG NM_001272041.1
Chemokine (C-C motif) ligand 4 *(Ccl4)* CTTCTGTGCTCCAGGGTTCTCA GCTCACTGGGGTTAGCACAGAT NM_013652.2
Chemokine (C-X3-C motif) ligand 1 *(Cx3cl1)* TGGCTTTGCTCATCCGCTATCAG CGTCTGTGCTGTGTCGTCTCC NM_009142.3
Chemokine (C-X-C motif) ligand 10 *(Cxcl10)* ATGACGGGCCAGTGAGAATG ATTCTTTTTCATCGTGGCAATGA NM_021274.2
Chemokine (C-X-C motif) ligand 16 *(Cxcl16)* CTTTATCAGGTTCCAGTTGCAGT CCCATGACCAGTTCCACACT NM_023158.7
Colony stimulating factor 1 (macrophage) *(Csf1)* CAGGAGTATTGCCAAGGAGGT GATCATCCAGCTGTTCCTGGTC NM_007778.4
Cyclophilin A *(Cphn)* AGCACTGGAGAGAAAGGATTTGG TCTTCTTGCTGGTCTTGCCATT NM_008907.1
Interleukin 1 beta *(Il1b)* TGCCACCTTTTGACAGTGATG TGATGTGCTGCTGCGAGATT NM_008361.4
Natriuretic peptide precursor type A *(Nppa)* ATGGGCTCCTTCTCCATCA CCTGCTTCCTCAGTCTGCTC NM_008725.3
Natriuretic peptide precursor type B *(Nppb)* GGATCTCCTGAAGGTGCTGT TTCTTTTGTGAGGCCTTGGT NM_008726.5
Ribosomal protein S16 *(Rps16)* TGCTGGTGTGGATATTCGGG CCTTGAGATGGGCTTATCGG NM_013647.2
Tumor necrosis factor *(Tnfa)* GATCGGTCCCCAAAGGGATG GTGGTTTGCTACGACGTGGG NM_013693.3

Supplemental Tables

Supplemental Table 1: Contractile function assessed by transthoracic echocardiography in WT, CIRS1KO and CIRS2KO mice (non-sedated mice)

Group (n)	Time post-surgery	HR [bpm] $	Area;d [mm²] #,$,&	Area;s [mm²] #,$,&	Majr;d [mm] #,$	Majr;s [mm] #	EDV [µl] #,$,&	ESV [µl] #,$,&	LV mass [mg] #,$	SV [µl] #,$	CO [ml/min] $	CI [ml/min/g] $	EF [%] #,$,&
WT Sham (6)	2 d	457.5 ± 57.9	11.12 ± 1.12	3.67 ± 0.74	7.29 ± 0.18	6.11 ± 0.24	68.2 ± 8.6	19.1 ± 4.3	85.6 ± 3.0	49.1 ± 5.3	21.6 ± 1.8	0.97 ± 0.10	73.3 ± 4.0
WT TAC (5)	2 d	507.2 ± 62.6	10.84 ± 1.46	5.95 ± 1.16	7.26 ± 0.39	6.02 ± 0.36	66.7 ± 11.1	30.9 ± 7.3	102.5 ± 9.1 †	35.8 ± 5.8	17.9 ± 3.5	0.87 ± 0.15	55.2 ± 5.1 †
CIRS1KO Sham (6)	2 d	422.2 ± 37.5	5.01 ± 0.58 *	1.11 ± 0.13	6.34 ± 0.27 *	5.14 ± 0.18	27.0 ± 4.1 *	4.8 ± 0.7	53.2 ± 2.9 *	22.2 ± 3.7 *	9.0 ± 1.2 *	0.60 ± 0.04 *	81.5 ± 1.9
CIRS1KO TAC (6)	2 d	419.3 ± 51.2	8.95 ± 0.92 †	6.05 ± 0.74 †	6.94 ± 0.19	6.21 ± 0.19 †	52.4 ± 6.7 †	31.6 ± 4.4 †	77.3 ± 4.4 *†	20.8 ± 3.0 *	8.4 ± 1.2 *	0.58 ± 0.07	39.7 ± 3.4 †
CIRS2KO Sham (6)	2 d	624.3 ± 64.0 ‡	8.17 ± 0.61	2.97 ± 0.72	6.77 ± 0.22	5.64 ± 0.36	46.5 ± 4.8	14.7 ± 4.6	71.2 ± 3.5 *‡	31.8 ± 1.6 *	19.9 ± 2.3 ‡	0.93 ± 0.11 ‡	70.9 ± 5.3
CIRS2KO TAC (7)	2 d	629.1 ± 33.4 ‡	13.01 ± 1.02 †‡	10.21 ± 1.38 *†‡	7.60 ± 0.18 †	6.66 ± 0.35 †	83.0 ± 7.9 †‡	58.3 ± 9.7 *†‡	101.2 ± 5.1 †‡	24.7 ± 2.1	15.5 ± 1.6 ‡	0.69 ± 0.06	32.9 ± 5.9 *†
Group (n)	**Time post-surgery**	**HR [bpm] $**	**Area;d [mm²] #,$**	**Area;s [mm²] #,$,&**	**Majr;d [mm] #,$**	**Majr;s [mm] #,$,&**	**EDV [µl] #,$,&**	**ESV [µl] #,$,&**	**LV mass [mg] #,$,&**	**SV [µl] $,&**	**CO [ml/min] $,&**	**CI [ml/min/g] &**	**EF [%] #,$,&**
WT Sham (9)	2 wk.	663.0 ± 19.0	5.38 ± 0.22	1.09 ± 0.06	6.39 ± 0.13	5.28 ± 0.17	28.7 ± 1.3	4.8 ± 0.2	68.8 ± 4.0	23.9 ± 1.3	15.8 ± 0.7	0.65 ± 0.11	83.2 ± 1.0
WT TAC (10)	2 wk.	660.0 ± 15.4	8.73 ± 0.98 †	3.67 ± 1.21	7.22 ± 0.15 †	6.14 ± 0.27 †	53.3 ± 6.9 †	20.6 ± 7.5	105.2 ± 5.4 †	32.7 ± 2.2 †	21.7 ± 1.7 †	0.93 ± 0.07 †	68.7 ± 7.1 †
CIRS1KO Sham (8)	2 wk.	708.6 ± 9.1	4.57 ± 0.32	0.99 ± 0.12	6.08 ± 0.15	4.83 ± 0.09	23.3 ± 2.1	4.0 ± 0.6	61.6 ± 4.4	19.3 ± 1.8	13.7 ± 1.3	0.67 ± 0.04	82.7 ± 1.7
CIRS1KO TAC (12)	2 wk.	722.4 ± 5.8 *	4.76 ± 0.27 *	0.95 ± 0.14 *	6.32 ± 0.09 *	5.13 ± 0.15 *	25.0 ± 1.3 *	4.1 ± 0.7 *	71.2 ± 3.3 *	20.8 ± 0.8 *	15.0 ± 0.6 *	0.76 ± 0.04 *	84.0 ± 1.9 *
CIRS2KO Sham (7)	2 wk.	662.3 ± 21.6	8.11 ± 0.65 ‡	2.1 ± 0.29	6.71 ± 0.13 ‡	5.40 ± 0.21	45.5 ± 4.3	9.7 ± 1.6	73.5 ± 4.5	35.9 ± 3.2 *‡	23.4 ± 1.5 *‡	0.91 ± 0.04 *‡	79.2 ± 2.4
CIRS2KO TAC (9)	2 wk.	580.2 ± 43.9 *‡	12.44 ± 1.68 *†‡	8.43 ± 1.71 *†‡	7.57 ± 0.25 †‡	6.89 ± 0.29 *†‡	80.0 ± 12.1 *†‡	51.3 ± 11.8 *†‡	125.7 ± 3.9 *†‡	28.8 ± 1.9 †‡	16.3 ± 1.1 *†	0.69 ± 0.06 *	43.4 ± 6.6 *†‡

Mice for the 2-d time point were operated at the age of 6 wk. (suture method, 27 G) and for the 2 wk. time point at 8 wk. (suture method, 27 G). Data shown are mean values ± SEM. Two-way ANOVA was performed to analyze differences after TAC surgery by genotype, followed by Holm-Šídák post-hoc analysis (# $p<0.05$ for TAC surgery, $ $p<0.05$ for genotype, and & $p<0.05$ for the interaction between TAC surgery and genotype). HR, heart rate; Area;d, left ventricular endocardial area at end-diastole (short axis view); Area;s, left ventricular endocardial area at end-systole (short axis view); Majr;d, left ventricular long-axis length at end-diastole (long axis view); Majr;s, left ventricular long-axis length at end-systole (long axis view); EDV, left ventricular end-diastolic volume; ESV, left ventricular end-systolic volume; SV, stroke volume; CO, cardiac output; CI, cardiac index; EF, ejection fraction. * $p<0.05$ vs. WT same surgery, † $p<0.05$ vs. Sham same genotype, ‡ $p<0.05$ vs. CIRS1KO same surgery.

Supplemental Table 2: Contractile function assessed by transthoracic echocardiography in WT, CIRS1KO and CIRS2KO mice (sedated mice)

Group (n)	Time post-surgery [wk.]	LVDd [mm] $	LVDs [mm] $	LVPWd [mm]	LVPWs [mm]	IVSd [mm]	IVSs [mm]	EF [%]	FS [%]	HR [bpm]	SV [µl] $	CO [ml/ml] $	CI [ml/min/g]
WT Sham (6)	0 wk.	3.75 ± 0.08	2.65 ± 0.10	0.69 ± 0.02	0.91 ± 0.02	0,79 ± 0,02	1,12 ± 0,04	64.9 ± 1.6	29.6 ± 1.1	464.9 ± 20.0	35.3 ± 1.1	16.3 ± 0.3	0.79 ± 0.04
WT TAC (15)	0 wk.	3.62 ± 0.10	2.49 ± 0.11	0.74 ± 0.02	1.00 ± 0.03	0,74 ± 0,01	1,02 ± 0,02	67.7 ± 1.6	31.7 ± 1.1	454.9 ± 17.4	34.5 ± 1.7	15.7 ± 0.9	0.77 ± 0.05
CIRS1KO Sham (6)	0 wk.	3.25 ± 0.06 *	2.20 ± 0.05	0.69 ± 0.03	0.94 ± 0.02	0,74 ± 0,02	1,04 ± 0,05	68.9 ± 1.2	32.3 ± 0.9	442.1 ± 19.6	26.5 ± 2.1 *	11.6 ± 0.8 *	0.84 ± 0.07
CIRS1KO TAC (18)	0 wk.	3.44 ± 0.07	2.41 ± 0.08	0.69 ± 0.01	0.92 ± 0.03 *	0,75 ± 0,02	1,02 ± 0,03	65.5 ± 1.8	30.3 ± 1.2	448.4 ± 9.9	28.9 ± 1.1 *	12.9 ± 0.5 *	0.81 ± 0.02
CIRS2KO Sham (6)	0 wk.	3.89 ± 0.08 ‡	2.70 ± 0.09	0.71 ± 0.03	0.99 ± 0.06	0,75 ± 0,02	1,07 ± 0,04	66.3 ± 2.5	30.6 ± 1.6	453.6 ± 31.0	40.3 ± 1.0 ‡	18.2 ± 1.0 ‡	0.87 ± 0.08
CIRS2KO TAC (17)	0 wk.	3.75 ± 0.10 ‡	2.66 ± 0.11	0.72 ± 0.02	0.97 ± 0.02	0,78 ± 0,02	1,07 ± 0,02	64.6 ± 1.7	29.6 ± 1.1	450.4 ± 18.8	34.1 ± 1.6 ‡	15.2 ± 0.8 ‡	0.74 ± 0.04
Group (n)	**Time post-surgery [wk.]**	**LVDd [mm] #,$**	**LVDs [mm] #,$**	**LVPWd [mm] #,$**	**LVPWs [mm] #,$**	**IVSd [mm]**	**IVSs [mm]**	**EF [%] #**	**FS [%] #**	**HR [bpm] #**	**SV [µl] $**	**CO [ml/ml] #,$**	**CI [ml/min/g] #**
WT Sham (10)	2 wk.	4.00 ± 0.07	2.86 ± 0.08	0.67 ± 0.02	0.90 ± 0.03	0.73 ± 0.02	1.04 ± 0.03	63.4 ± 1.6	28.7 ± 1.1	492.5 ± 15.1	42.0 ± 1.4	20.7 ± 1.0	0.87 ± 0.04
WT TAC (12)	2 wk.	4.01 ± 0.10	2.87 ± 0.10	0.76 ± 0.02 †	1.05 ± 0.03 †	0.78 ± 0.02	1.08 ± 0.04	63.1 ± 1.8	28.5 ± 1.2	515.2 ± 9.8	42.7 ± 2.4	22.0 ± 1.3	0.95 ± 0.05
CIRS1KO Sham (10)	2 wk.	3.52 ± 0.07 *	2.48 ± 0.06 *	0.62 ± 0.02	0.85 ± 0.04	0.73 ± 0.02	1.02 ± 0.03	65.0 ± 1.5	29.6 ± 1.0	480.5 ± 14.7	31.3 ± 1.7 *	15.1 ± 1.0 *	0.90 ± 0.06
CIRS1KO TAC (21)	2 wk.	3.85 ± 0.06 †	2.83 ± 0.08 †	0.67 ± 0.02 *	0.91 ± 0.02 *	0.73 ± 0.02	1.02 ± 0.03	60.4 ± 1.8	26.9 ± 1.1	515.2 ± 12.8	34.9 ± 1.2 *	18.0 ± 0.8 *	0.93 ± 0.03
CIRS2KO Sham (13)	2 wk.	4.01 ± 0.09 ‡	2.86 ± 0.09 ‡	0.67 ± 0.03	0.95 ± 0.05	0.72 ± 0.02	1.01 ± 0.03	63.7 ± 1.5	28.9 ± 1.0	509.1 ± 15.5	42.0 ± 2.0 ‡	21.4 ± 1.2 ‡	0.86 ± 0.04
CIRS2KO TAC (11)	2 wk.	4.24 ± 0.07 ‡	3.20 ± 0.06 *†‡	0.76 ± 0.02 †‡	0.98 ± 0.03	0.75 ± 0.01	0.99 ± 0.03	57.1 ± 1.4 †	24.7 ± 0.8 †	534.9 ± 9.3	44.5 ± 1.7 ‡	23.8 ± 1.0 ‡	0.96 ± 0.03
Group (n)	**Time post-surgery [wk.]**	**LVDd [mm] #,$**	**LVDs [mm] #,$**	**LVPWd [mm] #,$**	**LVPWs [mm] #**	**IVSd [mm] #**	**IVSs [mm] $**	**EF [%] #,$**	**FS [%] #,$**	**HR [bpm]**	**SV [µl] $**	**CO [ml/ml] $**	**CI [ml/min/g] &**
WT Sham (10)	4 wk.	4.00 ± 0.07	2.86 ± 0.09	0.68 ± 0.02	0.94 ± 0.03	0.72 ± 0.02	1.01 ± 0.04	63.5 ± 1.8	28.72 ± 1.3	512.3 ± 10.0	41.8 ± 1.4	21.4 ± 0.9	0.83 ± 0.03
WT TAC (12)	4 wk.	4.31 ± 0.14	3.25 ± 0.16	0.76 ± 0.02 †	1.02 ± 0.03	0.77 ± 0.02	1.02 ± 0.03	57.3 ± 2.6	25.09 ± 1.7	511.1 ± 15.0	44.5 ± 2.7	22.6 ± 1.3	0.93 ± 0.05
CIRS1KO Sham (10)	4 wk.	3.58 ± 0.05 *	2.48 ± 0.08	0.65 ± 0.01	0.91 ± 0.03	0.76 ± 0.02	1.07 ± 0.04	66.4 ± 2.3	30.85 ± 1.6	522.3 ± 21.4	34.1 ± 1.3 *	17.8 ± 0.9	1.01 ± 0.07 *
CIRS1KO TAC (21)	4 wk.	3.84 ± 0.10 *	2.75 ± 0.13 *	0.69 ± 0.02 *	0.95 ± 0.03	0.81 ± 0.02	1.14 ± 0.04 *	63.4 ± 2.6	29.14 ± 1.6	528.6 ± 15.9	35.1 ± 0.9 *	18.6 ± 0.7 *	0.92 ± 0.03
CIRS2KO Sham (13)	4 wk.	4.13 ± 0.08 ‡	2.94 ± 0.10 ‡	0.67 ± 0.02	0.95 ± 0.03	0.72 ± 0.02	1.03 ± 0.03	63.7 ± 1.9	28.94 ± 1.3	511.4 ± 14.5	44.6 ± 1.5 ‡	22.8 ± 0.9 ‡	0.84 ± 0.03 ‡
CIRS2KO TAC (11)	4 wk.	4.62 ± 0.07 *†‡	3.57 ± 0.07 †‡	0.75 ± 0.02 †‡	1.03 ± 0.03	0.77 ± 0.01	1.01 ± 0.03 ‡	53.8 ± 1.2†‡	22.72 ± 0.6 †‡	515.9 ± 17.1	48.2 ± 1.9 ‡	24.9 ± 1.4 ‡	0.97 ± 0.05

Mice were operated at the age of 6 wk. (clip method, 30 G). Data shown are mean values ± SEM. Two-way ANOVA was performed to analyze differences after TAC surgery by genotype, followed by Holm-Šídák post-hoc analysis (# $p<0.05$ for TAC surgery, $ $p<0.05$ for genotype, and & $p<0.05$ for the interaction between TAC surgery and genotype). LVDd, left ventricular cavity diameter at diastole; LVDs, left ventricular cavity diameter at systole; LVPWd, left ventricular posterior wall thickness at diastole; LVPWs, left ventricular posterior wall thickness at systole; IVSd, interventricular septum diameter at diastole; IVSs, interventricular septum diameter at systole; EF, Ejection fraction; FS, Fractional shortening; HR, heart rate; bpm, beats per minute; SV, stroke volume; CO, cardiac output; CI, cardiac index. * $p<0.05$ vs. WT same surgery, † $p<0.05$ vs. Sham same genotype, ‡ $p<0.05$ vs. CIRS1KO same surgery.

Supplemental Table 3: Characteristics of WT, CIRS1KO and CIRS2KO mice post-surgery

Group (n)	**Time post-surgery**	**BW [g] $**	**HW [mg] #,$,&**	**WLW [mg] #,$**	**HW/TL [mg/mm] #,$,&**	**WLW / TL [mg/mm] #,$**
WT Sham (6)	3 d	22.4 ± 0.6	114.0 ± 3.5	134.8 ± 5.9	6.83 ± 0.18	8.07 ± 0.31
WT TAC (8)	3 d	19.8 ± 0.8	160.5 ± 8.6 †	126.7 ± 7.4	9.86 ± 0.53 †	7.76 ± 0.41
CIRS1KO Sham (7)	3 d	15.3 ± 1.1 *	82.0 ± 7.9 *	105.8 ± 9.8	5.30 ± 0.48 *	6.87 ± 0.60
CIRS1KO TAC (6)	3 d	14.3 ± 0.9 *	91.3 ± 3.7 *	126.6 ± 9.7	5.91 ± 0.19 *	8.15 ± 0.49
CIRS2KO Sham (6)	3 d	21.5 ± 0.4 ‡	120.9 ± 2.8 ‡	135.7 ± 6.2	7.38 ± 0.17 ‡	8.28 ± 0.36
CIRS2KO TAC (7)	3 d	22.5 ± 0.5 *‡	163.2 ± 2.7 †‡	171.7 ± 11.2 *†‡	9.66 ± 0.18 †‡	10.16 ± 0.66 *†‡
Group (n)	**Time post-surgery**	**BW [g] $**	**HW [mg] #,$,&**	**WLW [mg] #,$,&**	**HW/TL [mg/mm] #,$,&**	**WLW / TL [mg/mm] #,$,&**
WT Sham (9)	2 wk.	24.3 ± 0.6	106.4 ± 3.2	143.2 ± 4.4	6.31 ± 0.19	8.49 ± 0.25
WT TAC (10)	2 wk.	23.3 ± 0.9	167.6 ± 7.6 †	222.8 ± 34.1 †	9.98 ± 0.46 †	13.26 ± 2.04 †
CIRS1KO Sham (8)	2 wk.	20.4 ± 0.8 *	101.3 ± 3.5	141.6 ± 10.6	6.31 ± 0.21	8.82 ± 0.66
CIRS1KO TAC (12)	2 wk.	20.1 ± 0.6 *	132.1 ± 4.2 *†	125.9 ± 4.3 *	8.31 ± 0.21 *†	7.94 ± 0.28 *
CIRS2KO Sham (7)	2 wk.	25.8 ± 1.1 ‡	116.5 ± 4.6	149.0 ± 6.4	6.79 ± 0.23	8.69 ± 0.37
CIRS2KO TAC (9)	2 wk.	24.1 ± 1.2 ‡	190.9 ± 6.1 *†‡	363.8 ± 42.0 *†‡	11.19 ± 0.36 *†‡	21.36 ± 2.47 *†‡
Group (n)	**Time post-surgery**	**BW [g] $**	**HW [mg] #,$,&**	**WLW [mg] #,$,&**	**HW/TL [mg/mm] #,$,&**	**WLW / TL [mg/mm] #,$,&**
WT Sham (10)	4 wk.	25.7 ± 0.6	112.9 ± 1.3	152.8 ± 4.5	6.49 ± 0.10	8.77 ± 0.22
WT TAC (10)	4 wk.	25.5 ± 0.5	170.7 ± 10.3 †	165.9 ± 7.6	10.02 ± 0.62 †	9.73 ± 0.45
CIRS1KO Sham (10)	4 wk.	18.3 ± 0.9 *	88.4 ± 3.6 *	121.3 ± 5.1 *	5.55 ± 0.17	7.61 ± 0.26
CIRS1KO TAC (10)	4 wk.	20.4 ± 0.5 *	106.9 ± 3.8 *†	129.9 ± 4.7 *	6.58 ± 0.22 *†	7.99 ± 0.24 *
CIRS2KO Sham (10)	4 wk.	26.2 ± 0.6 ‡	119.7 ± 2.7 ‡	152.1 ± 2.7 ‡	6.90 ± 0.15 ‡	8.77 ± 0.16
CIRS2KO TAC (10)	4 wk.	25.5 ± 0.6 ‡	198.3 ± 9.4 *†‡	208.3 ± 16.9 *†‡	11.55 ± 0.54 *†‡	12.14 ± 1.00 *†‡

Mice for the 3-d time point were operated at the age of 6 wk. (suture method, 27 G), for the 2 wk. time point at 8 wk. (suture method, 27 G), and for the 4 wk. time point at 6 wk. (clip method, 30 G). Data shown are mean values ± SEM. Two-way ANOVA was performed to analyze differences after TAC surgery by genotype, followed by Holm-Šídák post-hoc analysis (# $p<0.05$ for TAC surgery, $ $p<0.05$ for genotype, and & $p<0.05$ for the interaction between TAC surgery and genotype). BW, body weight; HW, heart weight; WLW, wet lung weight; TL, tibia length. * $p<0.05$ vs. WT same surgery, † $p<0.05$ vs. Sham same genotype, ‡ $p<0.05$ vs. CIRS1KO same surgery.

Supplemental Table 4: Invasive measurement of left ventricular pressures in WT, CIRS1KO and CIRS2KO mice four weeks post-surgery

Group (n)	**LVSP [mmHg]** #,$	**LVMP [mmHg]** #,&	**LV Dev P [mmHg]** #,$	**Max dP/dt [mmHg/s]** #,&	**Min dP/dt [mmHg/s]** #,&	**Heart Rate [bpm]**
WT Sham (10)	109.72 ± 4.23	3.88 ± 2.22	105.83 ± 2.98	8239 ± 604	-8639 ± 648	517 ± 32
WT TAC (10)	160.82 ± 2.19 †	7.75 ± 1.02	153.07 ± 2.73 †	6651 ± 359 †	-7244 ± 213 p=0.052 vs. WT TAC	508 ± 11
CIRS1KO Sham (9)	101.53 ± 3.00	6.56 ± 0.79	94.97 ± 2.86	6654 ± 325 *	-7408 ± 414	530 ± 17
CIRS1KO TAC (14)	135.43 ± 5.28 *†	6.17 ± 0.74	129.25 ± 5.18 *†	7112 ± 302	-8331 ± 359	523 ± 18
CIRS2KO Sham (11)	107.03 ± 4.17	2.52 ± 0.70	104.51 ± 4.28	8180 ± 506 ‡	-8209 ± 419	497 ± 17
CIRS2KO TAC (10)	149.59 ± 4.46 †‡	11.23 ± 1.36 †‡	138.35 ± 5.45 *†	5050 ± 309 *†‡	-6140 ± 356 †‡	514 ± 17

Mice were operated at the age of 6 wk. (clip method, 30 G). Data shown are mean values ± SEM. Two-way ANOVA was performed to analyze differences four weeks after TAC surgery by genotype, followed by Holm-Šídák post-hoc analysis (# $p<0.05$ for TAC surgery, $ $p<0.05$ for genotype, and & $p<0.05$ for the interaction between TAC surgery and genotype). LVSP, left ventricular systolic pressure; LVMP, left ventricular minimum pressure; LV Dev P, left ventricular developed pressure; Max dP/dt, maximal rate of increase in left ventricular pressure; Min dP/dt, maximal rate of decrease in left ventricular pressure; bpm, beats per minute. * $p<0.05$ vs. WT same surgery, † $p<0.05$ vs. Sham same genotype, ‡ $p<0.05$ vs. CIRS1KO same surgery.

Supplemental Table 5: Characteristics of CIRS2KO x Akt1^{het} cross mice four weeks post-surgery

Group	**BW pre-surgery [g]** **$**	**BW [g]** **$,&**	**HW [mg]** **#,$,&**	**WLW [mg]** **#,$**	**HW/TL [mg/mm]** **#,$,&**	**WLW / TL [mg/mm]** **#,$**
WT Sham	21.8 ± 0.7	25.0 ± 0.8	119.9 ± 4.2	170.9 ± 5.32	7.03 ± 0.22	10.02 ± 0.28
WT TAC	22.6 ± 0.3	25.3 ± 0.5	197.1 ± 14.7 *	259.2 ± 44.08 *	11.56 ± 0.87 *	15.22 ± 2.61 *
CIRS2KO Sham	23.9 ± 0.6 ‡	28.2 ± 1.0 ‡	126.0 ± 3.8	192.1 ± 4.65	7.16 ± 0.19	10.92 ± 0.23
CIRS2KO TAC	23.1 ± 0.4	26.7 ± 0.7	210.9 ± 8.6 *	301.5 ± 35.89 *	12.04 ± 0.52 *	17.22 ± 2.08 *
Akt1^{het} Sham	21.7 ± 0.6	25.0 ± 0.5	112.6 ± 2.4	169.3 ± 4.76	6.70 ± 0.14	10.07 ± 0.27
Akt1^{het} TAC	22.7 ± 0.5	25.5 ± 0.6	159.9 ± 8.1*†	201.8 ± 16.48	9.34 ± 0.46 *†	11.78 ± 0.95
CIRS2KO x Akt1^{het} Sham	22.2 ± 0.5	25.8 ± 0.8	117.5 ± 3.6	175.4 ± 3.43	6.81 ± 0.17	10.17 ± 0.15
CIRS2KO x Akt1^{het} TAC	23.6 ± 0.4	28.5 ± 0.4 *‡	167.2 ± 5.1 *†	189.7 ± 3.94 †	9.54 ± 0.29 *†	10.82 ± 0.21 †

Mice were operated at the age of 6 wk. (clip method, 30 G). Data shown are mean values ± SEM, n=10. Two-way ANOVA was performed to analyze differences four weeks after TAC surgery by genotype, followed by Holm-Šídák post-hoc analysis (# $p<0.05$ for TAC surgery, $ $p<0.05$ for genotype, and & $p<0.05$ for the interaction between TAC surgery and genotype). BW, body weight; HW, heart weight; WLW, wet lung weight; TL, tibia length. * $p<0.05$ vs. Sham same genotype, † $p<0.05$ vs. Akt1 WT same surgery, ‡ $p<0.05$ vs. IRS2 WT same surgery.

Supplemental Table 6: Contractile function assessed by transthoracic echocardiography in CIRS2KO x Akt1^{het} cross mice four weeks post-surgery (sedated mice)

Group	LVDd [mm] #,$	LVDs [mm] #,$,&	LVPWd [mm] #	LVPWs [mm] #	IVSd [mm] #	IVSs [mm] #,&	EF [%] #,&	FS [%] #,$,&	HR [bpm] #
WT Sham	3.96 ± 0.07	2.58 ± 0.15	0.80 ± 0.10	1.15 ± 0.11	0.76 ± 0.05	1.00 ± 0.06	49.5 ± 3.1	33.1 ± 2.3	425 ± 17
WT TAC	4.32 ± 0.12 *	3.39 ± 0.10 *	1.02 ± 0.08 *	1.34 ± 0.08	0.91 ± 0.07 *	0.99 ± 0.07	38.3 ± 3.3 *	20.7 ± 1.9 *	446 ± 21
CIRS2KO Sham	4.02 ± 0.08	2.67 ± 0.09	0.72 ± 0.06	1.17 ± 0.09	0.65 ± 0.04	0.85 ± 0.04	57.4 ± 3.0	32.9 ± 1.3	419 ± 16
CIRS2KO TAC	4.32 ± 0.11	3.61 ± 0.15 *	1.08 ± 0.08 *	1.28 ± 0.07	0.85 ± 0.05 *	0.96 ± 0.05	30.1 ± 3.6 *	15.9 ± 2.1 *	467 ± 10
Akt1^{het} Sham	3.93 ± 0.07	2.70 ± 0.12	0.75 ± 0.04	1.03 ± 0.09	0.75 ± 0.03	0.89 ± 0.05	49.6 ± 3.3	30.8 ± 2.6	410 ± 22
Akt1^{het} TAC	3.87 ± 0.11 †	2.74 ± 0.15 †	0.99 ± 0.08 *	1.39 ± 0.08 *	0.86 ± 0.03	1.15 ± 0.03 *	44.5 ± 2.9	29.5 ± 2.2 †	423 ± 15
CIRS2KO x Akt1^{het} Sham	3.94 ± 0.09	2.61 ± 0.11	0.74 ± 0.03	1.18 ± 0.04	0.66 ± 0.04	0.81 ± 0.04	54.7 ± 2.6	33.9 ± 1.4	427 ± 11
CIRS2KO x Akt1^{het} TAC	4.06 ± 0.06	2.90 ± 0.11 †	0.99 ± 0.05 *	1.35 ± 0.06	0.84 ± 0.05 *	1.07 ± 0.05 *	42.6 ± 2.3 *†	28.0 ± 1.9 †	447 ± 15

Mice were operated at the age of 6 wk. (clip method, 30 G). Data shown are mean values ± SEM, n=10. Two-way ANOVA was performed to analyze differences four weeks after TAC surgery by genotype, followed by Holm-Šídák post-hoc analysis (# $p<0.05$ for TAC surgery, $ $p<0.05$ for genotype, and & $p<0.05$ for the interaction between TAC surgery and genotype). LVDd, left ventricular cavity diameter at diastole; LVDs, left ventricular cavity diameter at systole; LVPWd, left ventricular posterior wall thickness at diastole; LVPWs, left ventricular posterior wall thickness at systole; IVSd, interventricular septum diameter at diastole; IVSs, interventricular septum diameter at systole; EF, Ejection fraction; FS, Fractional shortening; HR, heart rate; bpm, beats per minute. * $p<0.05$ vs. Sham same genotype, † $p<0.05$ vs. Akt1 WT same surgery.

Supplemental Table 7: Invasive measurement of left ventricular pressures in CIRS2KO x Akt1^{het} cross mice four weeks post-surgery

Group	LVSP [mmHg] #,$	LVMP [mmHg] #	LV Dev P [mmHg] #,$	Max dP/dt [mmHg/s] #,$	Min dP/dt [mmHg/s] #,$,&	Heart Rate [bpm]
WT Sham	100.00 ± 2.77	0.18 ± 0.88	99.82 ± 2.56	8985 ± 517	-9059 ± 385	495 ± 15
WT TAC	149.34 ± 5.53 *	7.00 ± 2.45 *	142.33 ± 6.51 *	6080 ± 469 *	-7156 ± 487 *	504 ± 21
CIRS2KO Sham	101.65 ± 1.69	1.01 ± 1.16	100.65 ± 1.32	8102 ± 323	-8656 ± 587	503 ± 12
CIRS2KO TAC	144.85 ± 6.71 *	9.27 ± 2.01 *	135.57 ± 8.47 *	5895 ± 560 *	-6669 ± 484 *	526 ± 22
Akt1^{het} Sham	102.26 ± 2.42	1.27 ± 0.76	101.00 ± 2.37	8401 ± 410	-8375 ± 466	494 ± 15
Akt1^{het} TAC	147.52 ± 3.40 *	4.02 ± 0.84	143.50 ± 3.43 *	6861 ± 214 *	-7765 ± 333	504 ± 12
CIRS2KO x Akt1^{het} Sham	105.68 ± 3.27	0.93 ± 0.71	104.75 ± 2.83	9370 ± 212	-9132 ± 308	515 ± 10
CIRS2KO x Akt1^{het} TAC	164.23 ± 4.63 *†‡	4.67 ± 1.27	159.56 ± 4.59 *†	7975 ± 557 *†	-9738 ± 703 †‡	509 ± 19

Mice were operated at the age of 6 wk. (clip method, 30 G). Data shown are mean values ± SEM, n=10. Two-way ANOVA was performed to analyze differences four weeks after TAC surgery by genotype, followed by Holm-Šídák post-hoc analysis (# $p<0.05$ for TAC surgery, $ $p<0.05$ for genotype, and & $p<0.05$ for the interaction between TAC surgery and genotype). LVSP, left ventricular systolic pressure; LVMP, left ventricular minimum pressure; LV Dev P, left ventricular developed pressure; Max dP/dt, maximal rate of increase in left ventricular pressure; Min dP/dt, maximal rate of decrease in left ventricular pressure; bpm, beats per minute. * $p<0.05$ vs. Sham same genotype, † $p<0.05$ vs. Akt1 WT same surgery, ‡ $p<0.05$ vs. IRS2 WT same surgery.

Supplemental Table 8: Patient characteristics

Parameter	Non-Failing	Failing
Number of patients [n]	7	17
Male / Female [n]	5/2	15/2
Age [years]	42.3 ± 2.7	61.6 ± 2.8 *
Body mass index [kg/m^2]	25.7 ± 1.2	28.9 ± 0.9
Body surface area [m^2]	1.9 ± 0.1	2.0 ± 0.1
Ischemic heart failure		41.2 %
NYHA class		3.9 ± 0.1
Ejection fraction [%]	63.2 ± 3.3	19.1 ± 1.8 *
Cardiac index [L/min/m^2]	4.3 ± 0.3	1.7 ± 0.1 *
LV mass [g]		310.7 ± 27.1
LV mass index [g/m^2]		156.7 ± 13.0
LV end-diastolic diameter [mm]	43.9 ± 1.9	68.7 ± 2.3 *
Type 1 Diabetes mellitus [%]	0	0
Type 2 Diabetes mellitus [%]	0	52.9%
noninsulin-dependent (NIDDM)	0	35.3%
insulin-dependent (IDDM)	0	17.6%

Data shown are mean values ± SEM, * $p<0.05$ vs. non-failing controls. LV mass was calculated using the Devereux and Reichek "cube" formula (15). No information is available for LV mass (reference range [g]: 88-224 for men and 67-162 for women) and for LV mass index (reference range [g/m^2]: 49-115 for men and 43-95 for women) for non-failing controls (16). Note that values for LV mass and LV mass index are available for only a total of 13 patients with terminal heart failure. For all other parameters, values are presented based on the information obtained from all 17 patients with end-stage heart failure.

Supplemental Table 9: Clustered heat map depicting the change in peptide phosphorylation four weeks post-surgery

ID	Sequence	Uniprot ID	Tyr	Ser	Thr	WT		CIRS1KO		CIRS2KO	
						Sham	TAC	Sham	TAC	Sham	TAC
KCC2G_278_289	VASMMHRQETVE	Q13555	Na	[280]	[287]						
BAD_112_124	RELRRMSDEFVDS	Q92934	Na	[118, 124]	[]						
pVASP_150_164	EHIERRV(pS)NAGGPPA	P50552	Na	[157]	[]						
pTY3H_64_78	RFIGRRQ(pS)LIEDARK	P07101	Na	[71]	[]						
ESR1_160_172	GGRERLASTNDKG	P03372	Na	[167]	[168]						
ADDB_696_708	GSPSKSPSKKKKK	P35612	Na	[697, 699, 701, 703]	[]						
AKT1_301_313	KDGATMKTFCGTP	P31749	Na	[]	[305, 308, 312]						
ELK1_356_368	LLPTHTLTPVLLT	P19419	Na	[]	[359, 361, 363, 368]						
P53_308_323	LPNNTSSSPQPKKKPL	P04637	Na	[313, 314, 315]	[312]						
AMPE_5_17	EREGSKRYCIQTK	Q07075	[12]	Na	Na						
VTNC_390_402	NQNSRRPSRATWL	P04004	Na	[393, 397]	[400]						
ART_025_CXGLRRWSLGGLRRWSL	GLRRWSLGGLRRWSL	Na	Na	Na	Na						
CREB1_126_138	EILSRRPSYRKIL	P16220	Na	[129, 133]	[]						
SCN7A_898_910	KNGCRRGSSLGQI	Q01118	Na	[905, 906]	[]						
RS6_228_240	IAKRRRLSSLRAS	P62753	Na	[235, 236, 240]	[]						
RYR1_4317_4329	VRRLRRLTAREAA	P21817	Na	[]	[4324]						
CSF1R_701_713	NIHLEKKYVRRDS	P07333	Na	[713]	[]						
MYPC3_268_280	LSAFRRTSLAGGG	Q14896	Na	[269, 275]	[274]						
GRIK2_708_720	FMSSRRQSVLVKS	Q13002	Na	[710, 711, 715, 720]	[]						
NCF1_321_333	QDAYRRNSVRFLQ	P14598	Na	[328]	[]						
KCNA6_504_516	ANRERRPSYLPTP	P17658	Na	[511]	[515]						
F263_454_466	NPLMRRNSVTPLA	Q16875	Na	[461]	[463]						
TOP2A_1463_1475	RRKRKPSTSDDSD	P11388	Na	[1469, 1471, 1474]	[1470]						
KAP3_107_119	NRFTRRASVCAEA	P31323	Na	[114]	[110]						
KAP2_92_104	SRFNRRVSVCAET	P13861	Na	[92, 99]	[104]						
NCF1_296_308	RGAPPRRSSIRNA	P14598	Na	[303, 304]	[]						
CFTR_761_773	LQARRRQSVLNLM	P13569	Na	[768]	[]						
E1A_ADE05_212_224	AILRRPTSPVSRE	P03255	Na	[219, 222]	[218]						
CDN1A_139_151	GRKRRQTSMTDFY	P38936	Na	[146]	[145, 148]						
ANXA1_209_221	AGERRKGTDVNVF	P04083	Na	[]	[216]						
PTN12_32_44	FMRLRRLSTKYRT	Q05209	Na	[39]	[40, 44]						
GBRB2_427_439	SRLRRRASQLKIT	P47870	Na	[427, 434]	[439]						
ERF_519_531	GEAGGPLTPRRVS	P50548	Na	[531]	[526]						
KIF2C_105_118_S106G	EGLRSRSTRMSTVS	Q99661	Na	[109, 111, 115, 118]	[112, 116]						
GYS2_1_13	MLRGRSLSVTSLG	P54840	Na	[6, 8, 11]	[10]						
BAD_93_105	FRGRSRSAPPNLW	Q92934	Na	[97, 99]	[]						
K6PL_766_778	LEHVTRRTLSMDK	P17858	Na	[775]	[770, 773]						
GPR6_349_361	QSKVPFRSRSPSE	P46095	Na	[350, 356, 358, 360]	[]						
FRAP_2443_2455	RTRTDSYSAGQSV	P42345	Na	[2448, 2450, 2454]	[2444, 2446]						
NOS3_1171_1183	SRIRTQSFSLQER	P29474	Na	[1171, 1177, 1179]	[1175]						
RB_242_254	AVIPINGSPRTPR	P06400	Na	[249]	[252]						
NMDZ1_890_902	SFKRRRSSKDTST	Q05586	Na	[890, 896, 897, 901]	[900, 902]						
PLEK_106_118	GQKFARKSTRRSI	P08567	Na	[113, 117]	[114]						
STK6_283_295	SSRRTTLCGTLDY	O14965	Na	[283, 284]	[287, 288, 292]						
NFKB1_330_342	FVQLRRKSDLETS	P19838	Na	[337, 342]	[341]						
CGHB_109_121	QCALCRRSTTDCG	P01233	Na	[116]	[117, 118]						
RAF1_253_265	QRQRSTSTPNVHM	P04049	Na	[257, 259]	[258, 260]						
PPR1A_28_40	QIRRRRPTPATLV	Q13522	Na	[]	[35, 38]						
ANDR_785_797	VRMRHLSQEFGWL	P10275	Na	[791]	[]						
NTRK3_824_836	LHALGKATPIYLD	Q16288	Na	[]	[831]						
BCKD_45_57	ERSKTVTSFYNQS	O14874	Na	[47, 52, 57]	[49, 51]						
PDE5A_95_107	GTPTRKISASEFD	O76074	Na	[102, 104]	[96, 98]						
NCF1_313_325	QRSRKRLSQDAYR	P14598	[324]	Na	Na						
ART_003_EAI(pY)AAPFAKKKXC	EAI(pY)AAPFAKKK	Na	Na	Na	Na						
RAF1_332_344	PRGQRDSSYYWEI	P04049	[340, 341]	Na	Na						
ART_004_EAIYAAPFAKKKXC	EAIYAAPFAKKK	Na	Na	Na	Na						
TYRO3_679_691	KIYSGDYYRQGCA	Q06418	[681, 685, 686]	Na	Na						
PDPK1_369_381	DEDCYGNYDNLLS	O15530	[373, 376]	Na	Na						
NTRK2_696_708	GMSRDVYSTDYYR	Q16620	[702, 706, 707]	Na	Na						
DCX_109_121	GIVYAVSSDRFRS	O43602	[112]	Na	Na						
RBL2_655_667	GLGRSITSPTTLY	Q08999	Na	[659, 662]	[661, 664, 665]						
MBP_222_234	HFFKNIVTPRTPP	P02686	Na	[]	[229, 232]						
NR4A1_344_356	GRRGRLPSKPKQP	P22736	Na	[351]	[]						
RAP1B_172_184	PGKARKKSSCQLL	P61224	Na	[179, 180]	[]						
BAD_69_81	IRSRHSSYPAGTE	Q92934	Na	[71, 74, 75]	[80]						
KCNA2_442_454	PDLKKSRSASTIS	P16389	Na	[447, 449, 451, 454]	[452]						
KPCB_19_31_A25S	RFARKGSLRQKNV	P05771	Na	[25]	[]						
H2B1B_27_40	GKKRKRSRKESYSI	P33778	Na	[33, 37, 39]	[]						
MP2K1_287_299	PPRPRTPGRPLSS	Q02750	Na	[298, 299]	[292]						
ACM5_498_510	CNRTFRKTFKMLL	P08912	Na	[]	[501, 505]						
MPIP1_172_184	FTQRQNSAPARML	P30304	Na	[178]	[173]						
ACM4_456_468	CNATFKKTFRHLL	P08173	Na	[]	[459, 463]						
ACM1_444_456	KIPKRPGSVHRTP	P11229	Na	[451]	[455]						
CENPA_1_14	MGPRRRSRKPEAPR	P49450	Na	[7]	[]						
ACM5_494_506	CYALCNRTFRKTF	P08912	Na	[]	[501, 505]						
PRKDC_2618_2630	TRTQEGSLSARWP	P78527	Na	[2624, 2626]	[2618, 2620]						
FOXO3_25_37	QSRPRSCTWPLQR	O43524	Na	[26, 30]	[32]						
VASP_271_283	LARRRKATQVGEK	P50552	Na	[]	[278]						
TEC_512_524	RYFLDDQYTSSSG	P42680	[513, 519]	Na	Na						
PGFRB_709_721	RPPSAELYSNALP	P09619	[716]	Na	Na						
K2C6B_53_65	GAGFGSRSLYGLG	P04259	[62]	Na	Na						
TAU_524_536	GSRSRTPSLPTPP	P10636	Na	[525, 527, 531]	[529, 534]						
GSUB_61_73	KKPRRKDTPALHI	O96001	Na	[]	[68]						
KCNB1_489_501	KWTKRTLSETSSS	Q14721	Na	[496, 499, 500, 501]	[491, 494, 498]						
LMNB1_16_28	GGPTTPLSPTRLS	P20700	Na	[23, 28]	[19, 20, 25]						
FIBA_569_581	EFPSRGKSSSYSK	P02671	Na	[572, 576, 577, 578, 580]	[]						
ERBB2_679_691	QQKIRKYTMRRLL	P04626	Na	[]	[686]						
ADDB_706_718	KKKFRTPSFLKKS	P35612	Na	[713, 718]	[711]						
H32_3_18	RTKQTARKSTGGKAPR	Q71DI3	Na	[11]	[4, 7, 12]						
IF4E_203_215	TATKSGSTTKNRF	P06730	Na	[207, 209]	[203, 205, 210, 211]						
MPIP3_208_220	RSGLYRSPSMPEN	P30307	Na	[209, 214, 216]	[]						
KPCB_626_639	AENFDRFFTRHPPV	P05771-2	Na	[]	[634]						
MARCS_152_164	KKKKKRFSFKKSF	P29966	Na	[159, 163]	[]						
KAPCG_192_206	VKGRTWTLCGTPEYL	P22612	Na	[]	[196, 198, 202]						
MARCS_160_172	FKKSFKLSGFSFK	P29966	Na	[163, 167, 170]	[]						
NEK3_158_170	FACTYVGTPYYVP	P51956	Na	[]	[161, 165]						
NEK2_172_184	FAKTFVGTPYYMS	P51955	Na	[184]	[175, 179]						

ID	Sequence	Uniprot ID	Tyr	Ser	Thr	WT		CIRS1KO		CIRS2KO	
						Sham	TAC	Sham	TAC	Sham	TAC
CDC2_154_169	GIPIRVYTHEVVTLWY	P06493	Na	[]	[161, 166]						
ACM1_421_433	CNKAFRDTFRLLL	P11229	Na	[]	[428]						
RB_803_815	NIYISPLKSPYKI	P06400	Na	[807, 811]	[]						
DCX_49_61	HFDERDKTSRNMR	O43602	Na	[57]	[56]						
KS6A1_374_386	QLFRGFSFVATGL	Q15418	Na	[380]	[384]						
CA2D1_494_506	LEDIKRLTPRFTL	P54289	Na	[]	[501, 505]						
P53_12_24	PPLSQETFSDLWK	P04637	Na	[15, 20]	[18]						
C1R_201_213	ASGYISSLEYPRS	P00736	Na	[202, 206, 207, 213]	[]						
CD27_212_224	HQRRKYRSNKGES	P26842	Na	[219, 224]	[]						
VGFR1_1326_1338	DYNSVVLYSTPPI	P17948	[1327, 1333]	Na	Na						
FAK1_569_581	RYMEDSTYYKASK	Q05397	[570, 576, 577]	Na	Na						
PGFRB_1014_1028	PNEGDNDYIIPLPDP	P09619	[1021]	Na	Na						
LAT_249_261	EEGAPDYENLQEL	O43561	[255]	Na	Na						
ANXA1_14_26	IENEEQEYVQTVK	P04083	[21]	Na	Na						
EPHB1_771_783	DDTSDPTYTSSLG	P54762	[778]	Na	Na						
LCK_387_399	RLIEDNEYTAREG	P06239	[394]	Na	Na						
EPHA7_607_619	TYIDPETYEDPNR	Q15375	[608, 614]	Na	Na						
JAK2_563_577	VRREVGDYGQLHETE	O60674	[570]	Na	Na						
FES_706_718	REEADGVYAASGG	P07332	[713]	Na	Na						
CD79A_181_193	EYEDENLYEGLNL	P11912	[182, 188]	Na	Na						
FRK_380_392	KVDNEDIYESRHE	P42685	[387]	Na	Na						
ENOG_37_49	SGASTGIYEALEL	P09104	[44]	Na	Na						
PGFRB_572_584	VSSDGHEYIYVDP	P09619	[579, 581]	Na	Na						
EPOR_361_373	SEHAQDTYLVLDK	P19235	[368]	Na	Na						
ZAP70_485_497	ALGADDSYYTARS	P43403	[492, 493]	Na	Na						
PDPK1_2_14	ARTTSQLYDAVPI	O15530	[9]	Na	Na						
FAK2_572_584	RYIEDEDYYKASV	Q14289	[573, 579, 580]	Na	Na						
MET_1227_1239	RDMYDKEYYSVHN	P08581	[1230, 1234, 1235]	Na	Na						
EFS_246_258	GGTDEGIYDVPLL	O43281	[253]	Na	Na						
41_654_666	LDGENIYIRHSNL	P11171	[660]	Na	Na						
SRC8_CHICK_492_504	YQAEENTYDEYEN	Q01406	[492, 499, 502]	Na	Na						
SRC8_CHICK_476_488	EYEPETVYEVAGA	Q01406	[477, 483]	Na	Na						
CDK2_8_20	EKIGEGTYGVVYK	P24941	[15, 19]	Na	Na						
PECA1_706_718	KKDTETVYSEVRK	P16284	[713]	Na	Na						
RASA1_453_465	TVDGKEIYNTIRR	P20936	[460]	Na	Na						
RET_1022_1034	TPSDSLIYDDGLS	P07949	[1029]	Na	Na						
P85A_600_612	NENTEDQYSLVED	P27986	[607]	Na	Na						
EPHA2_765_777	EDDPEATYTTSGG	P29317	[772]	Na	Na						
EPHA1_774_786	LDDFDGTYETQGG	P21709	[781]	Na	Na						
VGFR2_989_1001	EEAPEDLYKDFLT	P35968	[996]	Na	Na						
FER_707_719	RQEDGGVYSSSGL	P16591	[714]	Na	Na						
PLCG1_764_776	IGTAEPDYGALYE	P19174	[771, 775]	Na	Na						
PAXI_111_123	VGEEEHVYSFPNK	P49023	[118]	Na	Na						
RON_1346_1358	SALLGDHYVQLPA	Q04912	[1353]	Na	Na						
MK12_178_190	ADSEMTGYVVTRW	P53778	[185]	Na	Na						
VGFR2_1168_1180	AQQDGKDYIVLPI	P35968	[1175]	Na	Na						
JAK1_1015_1027	AIETDKEYYTVKD	P23458	[1022, 1023]	Na	Na						
KPB1_1011_1023	QVEFRRLSISAES	P46020	Na	[1018, 1020, 1023]	[]						
CFTR_730_742	EPLERRLSLVPDS	P13569	Na	[737, 742]	[]						
TY3H_65_77	FIGRRQSLIEDAR	P07101	Na	[71]	[]						
VASP_150_162	EHIERRVSNAGGP	P50552	Na	[157]	[]						
PLM_76_88	EEGTFRSSIRRLS	O00168	Na	[82, 83, 88]	[79]						
EPB42_241_253	LLNKRRGSVPILR	P16452	Na	[248]	[]						
CAC1C_1974_1986	ASLGRRASFHLEC	Q13936	Na	[1975, 1981]	[]						
ADRB2_338_350	ELLCLRRSSLKAY	P07550	Na	[345, 346]	[]						
LIPS_944_956	GFHPRRSSQGATQ	Q05469	Na	[950, 951]	[955]						
PTK6_436_448	ALRERLSSFTSYE	Q13882	Na	[442, 443, 446]	[445]						
STMN2_90_102	AAGERRKSQEAQV	Q93045	Na	[97]	[]						
REL_260_272	KMQLRRPSDQEVS	Q04864	Na	[267, 272]	[]						
KCNA3_461_473	EELRKARSNSTLS	P22001	Na	[468, 470, 473]	[471]						
GPSM2_394_406	PKLGRRHSMENME	P81274	Na	[401]	[]						
KCNA1_438_450	DSDLSRRSSSTMS	Q09470	Na	[439, 442, 445, 446, 447, 450]	[448]						
DESP_2842_2854	RSGSRRGSFDATG	P15924	Na	[2843, 2845, 2849]	[2853]						
MK10_216_228	TSFMMTPYVVTRY	P53779	[223, 228]	Na	Na						
VGFR2_1052_1064	DIYKDPDYVRKGD	P35968	[1054, 1059]	Na	Na						
MK01_180_192	HTGFLTEYVATRW	P28482	[187]	Na	Na						
PRRX2_202_214	WTASSPYSTVPPY	Q99811	[208, 214]	Na	Na						
CDK7_157_169	GLAKSFGSPNRAY	P50613	[169]	Na	Na						
CDK7_163_175	GSPNRAYTHQVVT	P50613	Na	[164]	[170, 175]						
EPHB4_583_595	IGHGTKVYIDPFT	P54760	[590]	Na	Na						
EPHB1_921_933	SAIKMVQYRDSFL	P54762	[928]	Na	Na						
ZBT16_621_633	LRTHNGASPYQCT	Q05516	[630]	Na	Na						
FGFR2_762_774	TLTTNEEYLDLSQ	P21802	[769]	Na	Na						
NPT2A_501_513	AKALGKRTAKYRW	Q06495	[511]	Na	Na						
MBP_198_210	ARTAHYGSLPQKS	P02686	[203]	Na	Na						
EPOR_419_431	ASAASFEYTILDP	P19235	[426]	Na	Na						
MBP_259_271	FGYGGRASDYKSA	P02686	[261, 268]	Na	Na						
CTNB1_79_91	VADIDGQYAMTRA	P35222	[86]	Na	Na						
VGFR3_1061_1073	DIYKDPDYVRKGS	P35916	[1063, 1068]	Na	Na						
VGFR2_944_956	RFRQGKDYVGAIP	P35968	[951]	Na	Na						

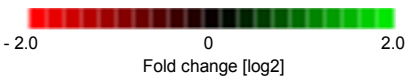

Changes are presented relative to Sham controls same genotype. Red indicates decreased signal intensity, green indicates increased signal intensity.

Supplemental Table 10: Prediction for activated upstream kinases four weeks post-TAC surgery

	UniProt ID	Hits	% Hits	Comb. Score
WT TAC				
mTOR/FRAP	P42345	1.000	50.01	228.4
PKG1 (PRKG1)	Q13976	0.667	33.34	319.1
PKACa (PRKACA)	P17612	0.667	33.34	314.2
PKACb (PRKACB)	P22694	0.667	33.34	314.2
Akt1 (PKBa)	P31749	0.667	33.34	250.4
SGK2	Q9HBY8	0.667	33.34	198.9
CIRS1KO TAC				
PKG2 (PRKG2)	Q13237	14.580	56.08	6535.0
PKG1 (PRKG1)	Q13976	13.247	50.95	6020.4
Pim3 (AL549548)	P58750	11.416	43.91	6767.1
MAPKAPK3	Q16644	10.500	40.38	5061.0
Pim1	P11309	10.416	40.06	7000.2
PRKX	P51817	9.415	36.21	4462.5
PKACa (PRKACA)	P17612	8.915	34.29	4264.8

Significantly altered peptides were queried against the proprietary upstream kinase predictor from Kinexus (www.phosphonet.ca). No upstream kinase activation was predicted for CIRS2KO hearts post-TAC surgery.

Supplemental Figures

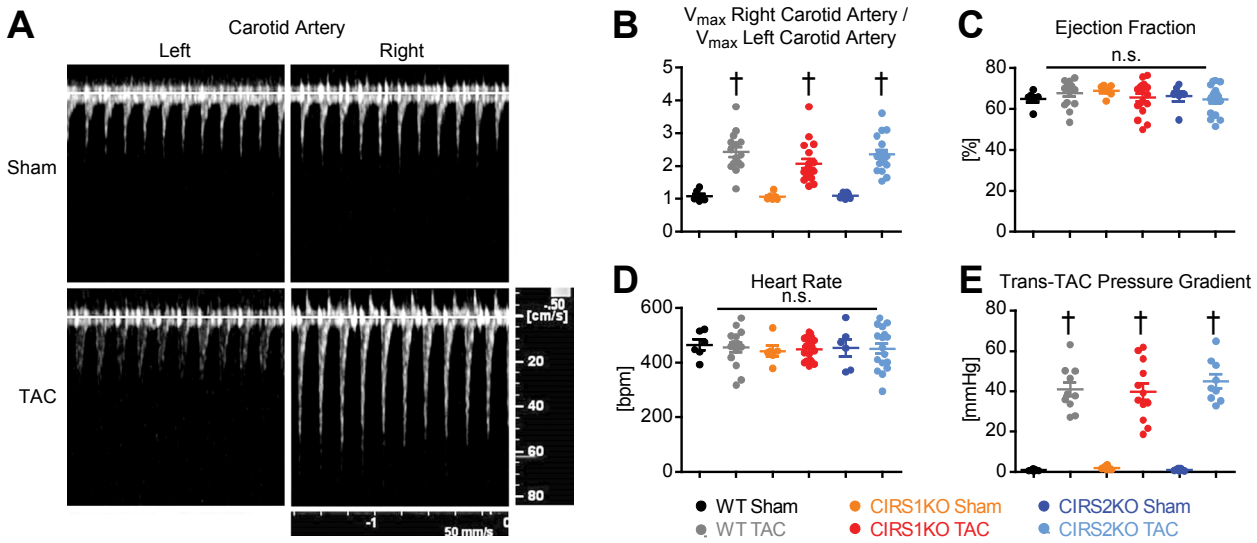

Supplemental Figure 1: *Transverse aortic constriction (TAC) results in a similar increase in the pressure gradient independent of the genotype.*
Two-way ANOVA was performed to analyze differences after TAC surgery by genotype, followed by Holm-Šídák post-hoc analysis (# $p<0.05$ for TAC surgery). (A) Representative images and (B) quantification of the measurements of peak velocity (V_{max}) of the left and right carotid artery immediately post Sham or TAC surgery (#) as indicated. (C) Ejection fraction and (D) heart rate determined by transthoracic echocardiography immediately post Sham or TAC surgery (same echocardiographic data as presented in Supplemental Table 2); n=6 for Sham groups, n=15-18 for TAC groups. † $p<0.05$ vs. Sham same genotype. (E) TAC-induced pressure gradient as determined by pulsed-wave Doppler measurement of transverse aortic velocity distal the constriction, n=11-14. Two-way ANOVA was performed to analyze differences after TAC surgery by genotype, followed by Holm-Šídák post-hoc analysis. Data shown are mean values ± SEM; n.s., no significant difference observed.

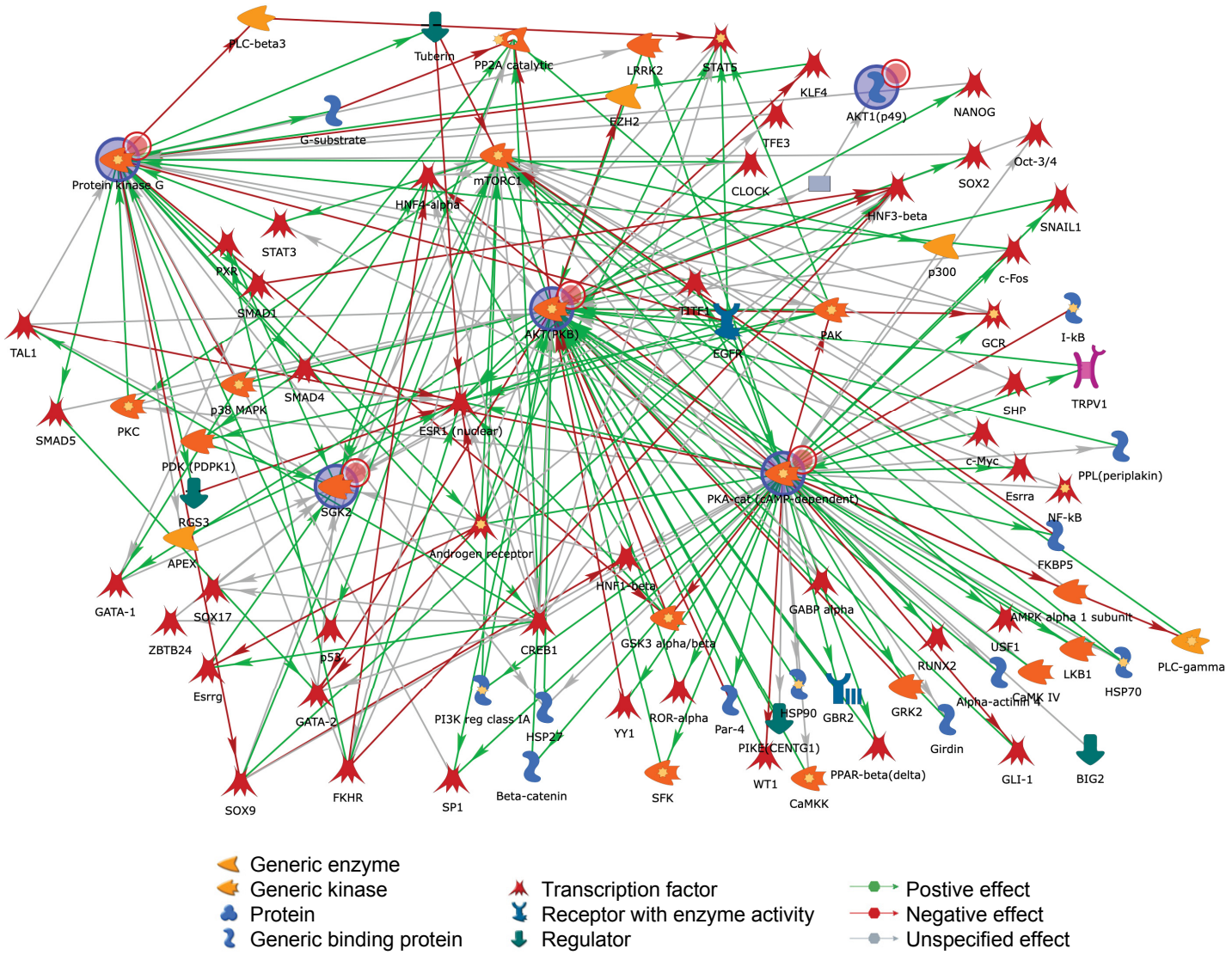

Supplemental Figure 2: *3-step network for TAC regulated kinase pathways in WT hearts relative to Sham controls four weeks post-surgery.*

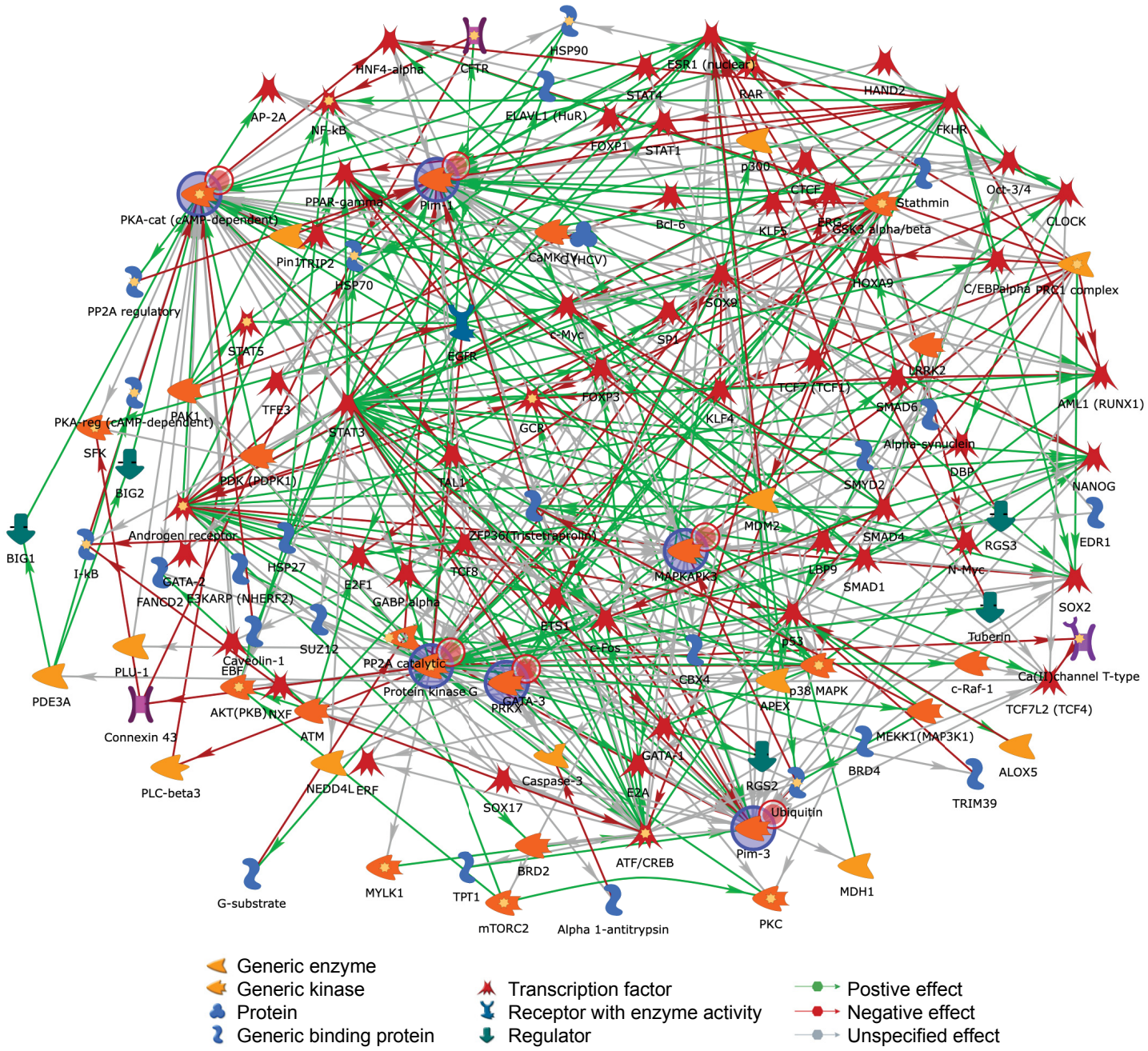

Supplemental Figure 3: *3-step network for TAC regulated kinase pathways in CIRS1KO hearts relative to Sham controls four weeks post-surgery.*

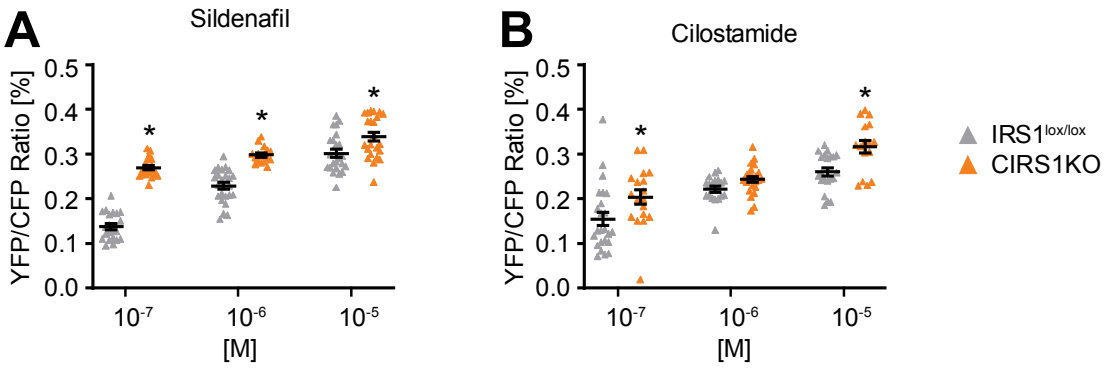

Supplemental Figure 4: *ANP stimulated cGMP production in the presence of the PDE5 inhibitor Sildenafil and the PDE3 inhibitor Cilostamide.*
ANP stimulated cGMP production in cardiomyocytes obtained from IRS1$^{lox/lox}$ and CIRS1KO mice measured by using the FRET-based cGMP sensor cGi-500 with or without varying concentrations of the (A) PDE5 inhibitor Sildenafil and (B) the PDE3 inhibitor Cilostamide. n=3-5 mice, n=16-25 cells / group total analyzed. Two-way ANOVA analysis was performed ($p<0.05$ for genotype, treatment and interaction between genotype and treatment) followed by Holm-Šídák post-hoc analysis, * $p<0.05$ vs. IRS1$^{lox/lox}$ same inhibitor concentration. Data shown are mean values ± SEM.

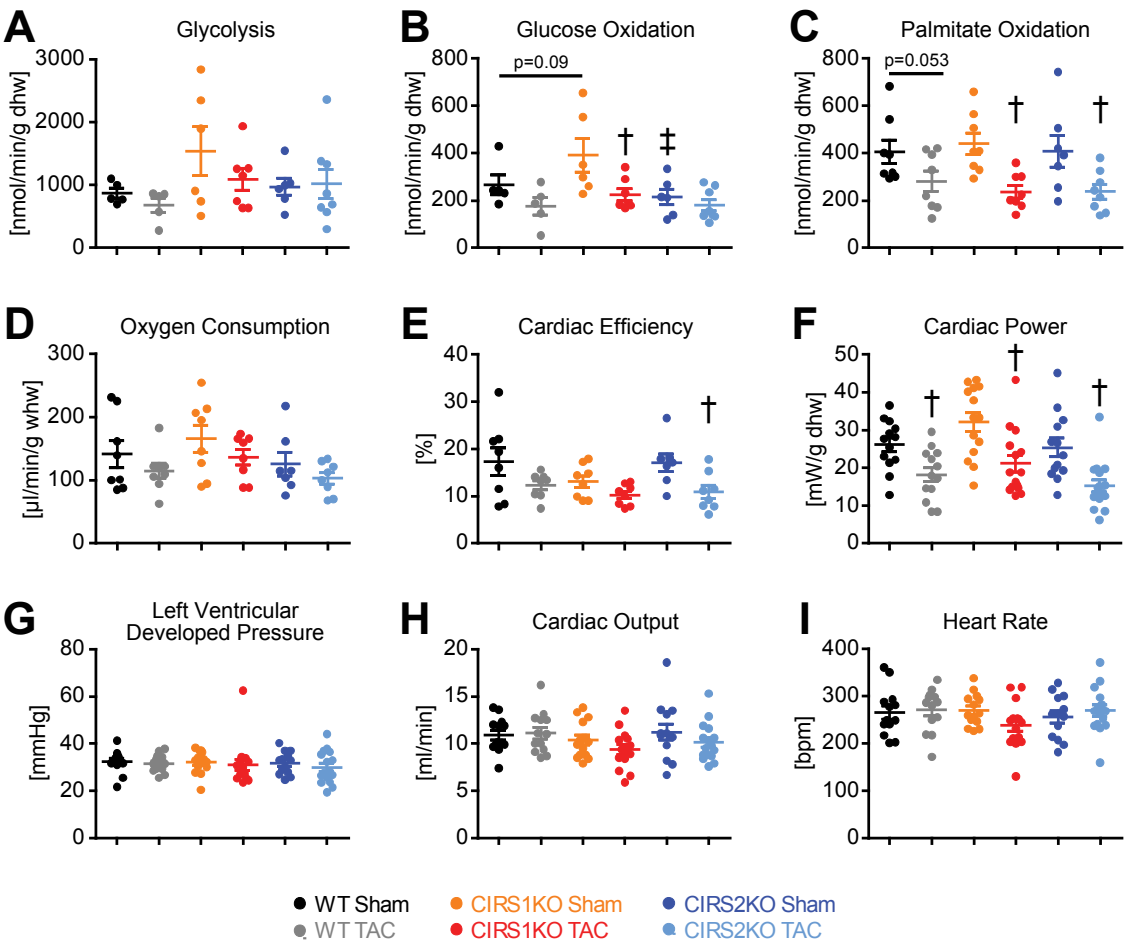

Supplemental Figure 5: *Cardiac substrate metabolism and function in isolated working WT, CIRS1KO and CIRS2KO hearts four weeks post-surgery.*
Two-way ANOVA was performed to analyze differences by four weeks after TAC surgery and genotype, followed by Holm-Šídák post-hoc analysis (# $p<0.05$ for TAC surgery, $ $p<0.05$ for genotype, and & $p<0.05$ for the interaction between TAC surgery and genotype). (A) Glycolysis, (B) glucose oxidation (#,$), (C) palmitate oxidation (#), (D) oxygen consumption, (E) cardiac efficiency (#), (F) cardiac power (#,$), (G) developed pressure, (H) cardiac output, and (I) heart rate (&). Data shown are mean values ± SEM. † $p<0.05$ vs. Sham same genotype. n=5-8 hearts per group for metabolism, oxygen consumption and cardiac efficiency; n=13-16 for cardiac function (pooled data from glucose and palmitate perfusions).

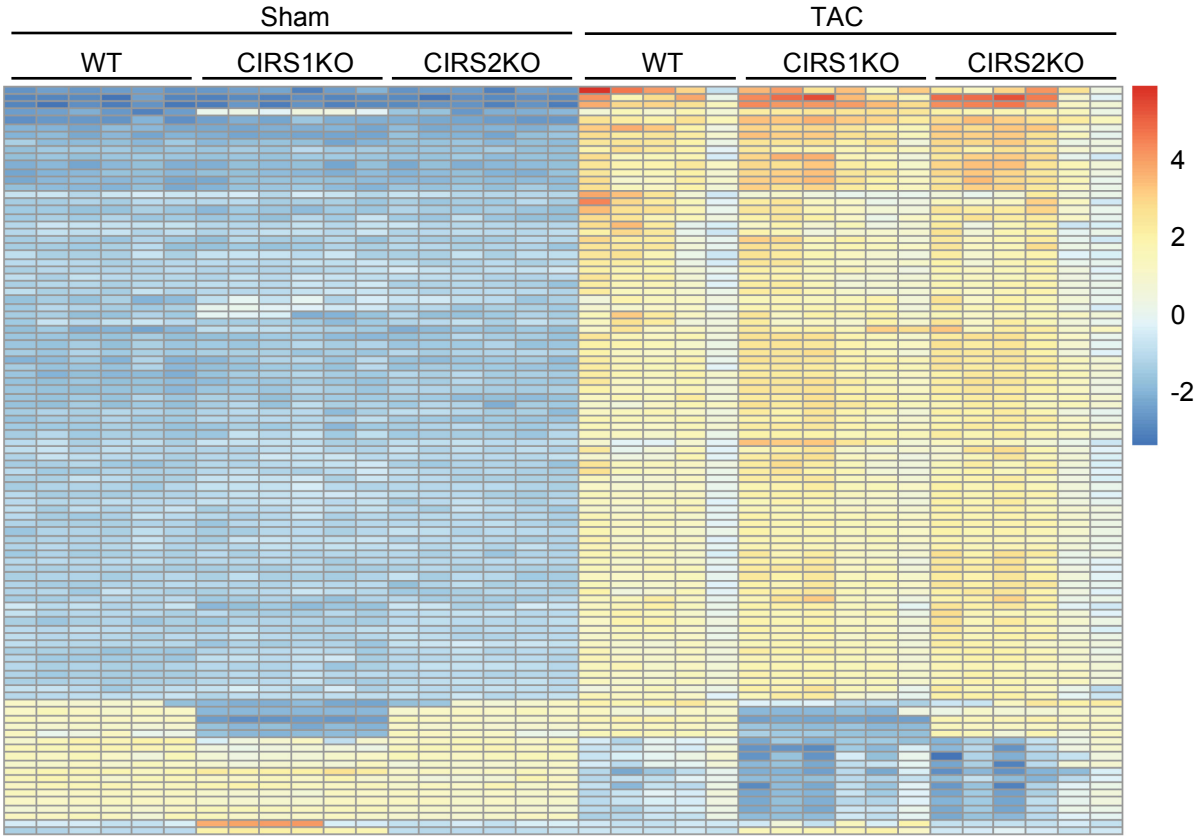

Supplemental Figure 6: *RNA sequencing quality control three days post-surgery.*
Heatmap of RNA sequencing count data corresponding to 100 genes with the greatest variance across samples. Data is clustered by row after applying the regularized log transformation function in DESeq2.

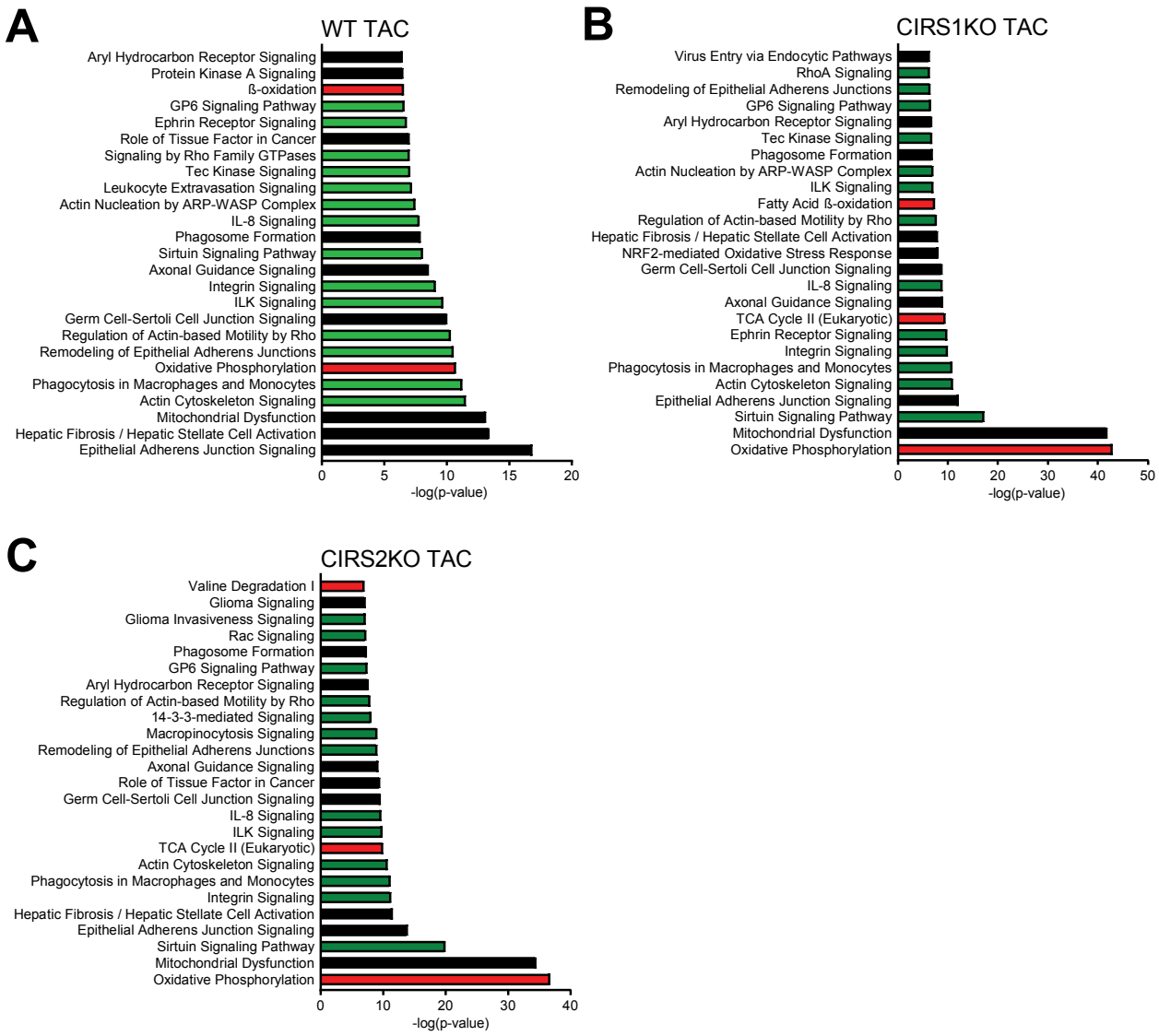

Supplemental Figure 7: *Common and unique pathways regulated in WT, CIRS1KO and CIRS2KO hearts three days post-TAC.*

Ingenuity pathway analysis indicates both common and unique pathways are enriched in WT (A), CIRS1KO (B), and CIRS2KO (C) TAC data sets. Several pathways are predicted to be inhibited (red, Z-score ≤ -2) or activated (green, Z-score ≥ 2).

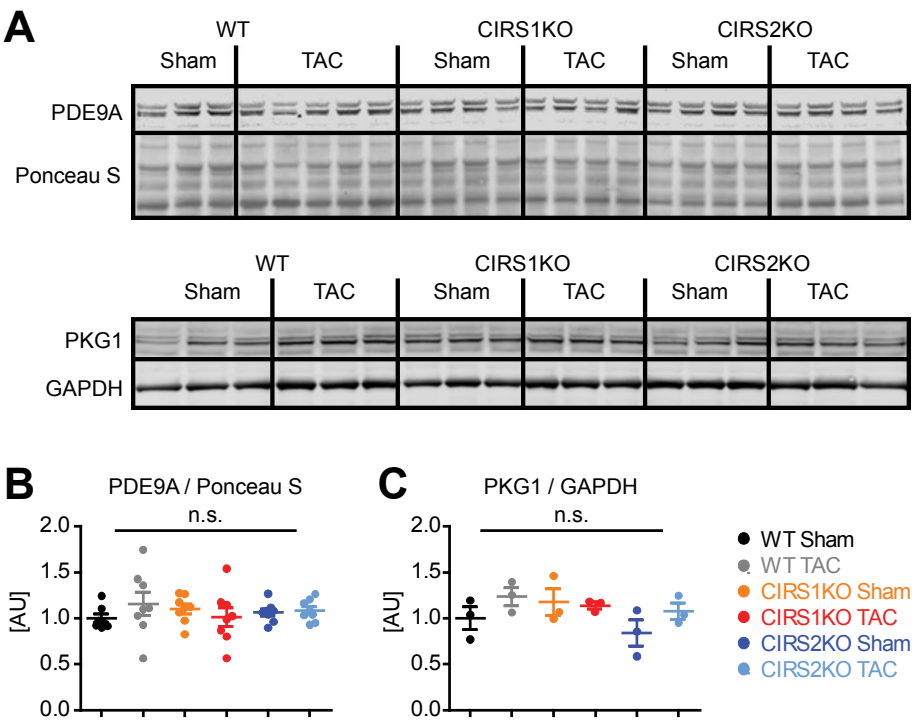

Supplemental Figure 8: (A) Representative immunoblots in ventricle homogenates of WT, CIRS1KO and CIRS2KO mice post-TAC surgery and densitometric quantification of (B) PDE9A normalized to Ponceau S (n=7-8), (C) PKG1 normalized to GAPDH (n=3). Two-way ANOVA was performed to analyze differences four weeks after TAC surgery by genotype, followed by Holm-Šídák post-hoc analysis. n.s., no significant difference observed. Data shown are mean values ± SEM.

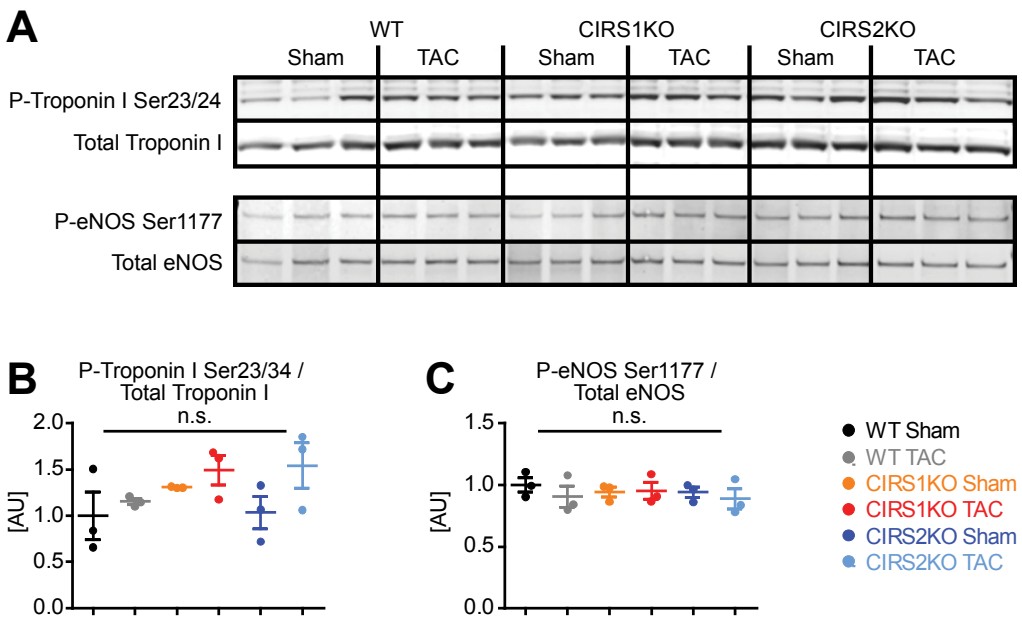

Supplemental Figure 9: (A) Representative immunoblots in ventricle homogenates of WT, CIRS1KO and CIRS2KO mice post-TAC surgery and densitometric quantification of (B) P-Troponin I Ser23/24 / Total Troponin I (n=3), (C) P-eNOS Ser1177 / Total eNOS (n=3). Two-way ANOVA was performed to analyze differences four weeks after TAC surgery by genotype, followed by Holm-Šídák post-hoc analysis. n.s., no significant difference observed. Data shown are mean values ± SEM.

Supplemental References

1. Pereira RO, Wende AR, Crum A, Hunter D, Olsen CD, Rawlings T, et al. Maintaining PGC-1alpha expression following pressure overload-induced cardiac hypertrophy preserves angiogenesis but not contractile or mitochondrial function. *FASEB journal : official publication of the Federation of American Societies for Experimental Biology.* 2014;28(8):3691-702.
2. Riehle C, Wende AR, Zaha VG, Pires KM, Wayment B, Olsen C, et al. PGC-1beta deficiency accelerates the transition to heart failure in pressure overload hypertrophy. *Circ Res.* 2011;109(7):783-93.
3. Bhan A, Sirker A, Zhang J, Protti A, Catibog N, Driver W, et al. High-frequency speckle tracking echocardiography in the assessment of left ventricular function and remodeling after murine myocardial infarction. *American journal of physiology Heart and circulatory physiology.* 2014;306(9):H1371-83.
4. El Accaoui RN, Gould ST, Hajj GP, Chu Y, Davis MK, Kraft DC, et al. Aortic valve sclerosis in mice deficient in endothelial nitric oxide synthase. *American journal of physiology Heart and circulatory physiology.* 2014;306(9):H1302-13.
5. Hill JA, Karimi M, Kutschke W, Davisson RL, Zimmerman K, Wang Z, et al. Cardiac hypertrophy is not a required compensatory response to short-term pressure overload. *Circulation.* 2000;101(24):2863-9.
6. Li YH, Reddy AK, Ochoa LN, Pham TT, Hartley CJ, Michael LH, et al. Effect of age on peripheral vascular response to transverse aortic banding in mice. *The journals of gerontology Series A, Biological sciences and medical sciences.* 2003;58(10):B895-9.
7. Baumgarten G, Knuefermann P, Kalra D, Gao F, Taffet GE, Michael L, et al. Load-dependent and -independent regulation of proinflammatory cytokine and cytokine receptor gene expression in the adult mammalian heart. *Circulation.* 2002;105(18):2192-7.
8. Mohammed SF, Storlie JR, Oehler EA, Bowen LA, Korinek J, Lam CS, et al. Variable phenotype in murine transverse aortic constriction. *Cardiovascular pathology : the official journal of the Society for Cardiovascular Pathology.* 2012;21(3):188-98.
9. Mandarim-de-Lacerda CA. Stereological tools in biomedical research. *An Acad Bras Cienc.* 2003;75(4):469-86.
10. Anderson JC, Duarte CW, Welaya K, Rohrbach TD, Bredel M, Yang ES, et al. Kinomic exploration of temozolomide and radiation resistance in Glioblastoma multiforme xenolines. *Radiotherapy and oncology : journal of the European Society for Therapeutic Radiology and Oncology.* 2014;111(3):468-74.
11. Jarboe JS, Jaboin JJ, Anderson JC, Nowsheen S, Stanley JA, Naji F, et al. Kinomic profiling approach identifies Trk as a novel radiation modulator. *Radiotherapy and oncology : journal of the European Society for Therapeutic Radiology and Oncology.* 2012;103(3):380-7.
12. Anderson JC, Minnich DJ, Dobelbower MC, Denton AJ, Dussaq AM, Gilbert AN, et al. Kinomic profiling of electromagnetic navigational bronchoscopy specimens: a new approach for personalized medicine. *PloS one.* 2014;9(12):e116388.
13. Love MI, Huber W, and Anders S. Moderated estimation of fold change and dispersion for RNA-seq data with DESeq2. *Genome Biol.* 2014;15(12):550.
14. Anders S, Pyl PT, and Huber W. HTSeq--a Python framework to work with high-throughput sequencing data. *Bioinformatics.* 2015;31(2):166-9.
15. Devereux RB, Alonso DR, Lutas EM, Gottlieb GJ, Campo E, Sachs I, et al. Echocardiographic assessment of left ventricular hypertrophy: comparison to necropsy findings. *The American journal of cardiology.* 1986;57(6):450-8.
16. Lang RM, Bierig M, Devereux RB, Flachskampf FA, Foster E, Pellikka PA, et al. Recommendations for chamber quantification: a report from the American Society of Echocardiography's Guidelines and Standards Committee and the Chamber Quantification Writing Group, developed in conjunction with the European Association of Echocardiography, a branch of the European Society of Cardiology. *Journal of the American Society of Echocardiography : official publication of the American Society of Echocardiography.* 2005;18(12):1440-63.